X-ray Absorption Spectroscopic Studies on Model Compounds for Biological Iodine and Bromine

Martin C. Feiters,[1] Frithjof C. Küpper,[2,3,#] and Wolfram Meyer-Klaucke[4]

-1- Department of Organic Chemistry, Institute of Molecules and Materials (IMM), Radboud University Nijmegen, 1 Toernooiveld, NL-6525 ED Nijmegen, The Netherlands
-2- Department of Chemistry and Biochemistry, University of California, Santa Barbara, CA 93106, USA
-3- Universität Konstanz, Fachbereich Biologie, D-78457 Konstanz, Germany
-4- European Molecular Biology Laboratory (EMBL), DESY, Notkestrasse 85, D-22603 Hamburg, Germany

Present address: The Scottish Association for Marine Science, Dunstaffnage Marine Laboratory, Oban, Argyll PA 37 1QA, Scotland, United Kingdom

Abstract

We have measured the X-ray absorption spectra of a number of organic iodine and bromine compounds of biological relevance, as well as of a series of iodine compounds with different oxidation states. We find that the iodine K edge spectra (XANES) are relatively featureless but that the position of the edge is sensitive to formal valence (among other factors), and the edge shape to the number of bound oxygens. EXAFS spectra of organohalogen compounds (both iodine and bromine) can be used to discriminate between aliphatic and aromatic compounds. There are differences both in the distances from the halogens to the first shell of carbons, which are shorter for aromatic compounds, as well as in the patterns of shells in the Fourier transforms. This result is expected to be relevant to studies at these edges in biological systems.

Abbreviations: EXAFS = extended X-ray absorption fine structure; XANES = X-ray absorption near-edge structure; XAS = X-ray absorption spectroscopy

Introduction

In recent years, X-ray absorption spectroscopy has been applied to elucidate the chemistry of an increasing variety of elements in biological systems, initially mainly relatively abundant transition metals in metalloproteins (Cramer 1988), more recently also trace elements like Sr (Greegor et al., 1997) or Hg (Harris et al., 2003), also including non-metals like S (Pickering et al., 1998; Pickering et al., 2001) and Se (Pickering et al., 1999; Lee et al., 2001). We have recently started studies on the halogen metabolism of brown algae, in which we expect to be able to establish both the chemical environment as well as the formal oxidation state of iodine and bromine under a number of physiologically relevant circumstances. We report here on our preparatory study on a number of model compounds relevant to the biological studies by which we explore the potential of the X-ray absorption technique to identify both chemical environments and oxidation states of iodine and bromine. The compounds were selected with the specific problem of halogen metabolism by brown algae in mind but are expected to have relevance to other future biological X-ray absorption studies at the iodine and bromine K-edges.

- - - FIGURE 1 - - -

The current view on the biogeochemical cycle of iodine is schematically represented in Figure 1. The most important role of iodine in mammals is in the thyroid hormones thyroxine and T3, which are both iodinated tyrosine derivatives that are interconverted by iodination/deiodination, and play a role in regulating the basal metabolism rate. Iodine occurs in seawater mainly as iodate but is reduced to iodide possibly through the action of nitrate reductase in bacteria and phytoplankton (Farrenkopf et al., 1997; Wong et al., 2002). In this form it is actively accumulated by brown algae like *Laminaria digitata* by a factor of 10^6 to a concentration as high as 73 mM through the action of vanadium haloperoxidase, requiring hydrogen peroxide as a cosubstrate (Küpper et al., 1998). Not surprisingly, iodine was first identified as an element early in the 19^{th} century (Courtois, 1813) in the ashes of these brown algae (kelp). Laminariales can be considered a major contributor to the biogeochemical pump of iodine from the ocean to the atmosphere (Carpenter et al., 2000) as they are very active in the so-called iodovolatilization, i.e. the incorporation of iodine in volatile organoiodine compounds. The established role of haloperoxidase, which can both oxidize halides to the hypohalous acid level as well as incorporate halogens in organic substrates (for review: Butler

et al., 2001) in the accumulation of iodine (Küpper et al., 1998) raises the question in what form it is stored in algae, possibly in specialized organelles. The question of the chemical form of accumulated iodine in brown algae had evoked interest already in the 19th century, but is still controversial despite a number of studies. Eschle (1897) reported that iodine in *Laminaria* is present "almost exclusively" in organic form. In contrast, Kylin (1929) suggested that in *Laminaria*, iodine was present mainly as iodide, but presumed also the existence of organically bound iodine. Roche & Yagi (1952) proposed that the iodine was present as iodotyrosines, which are potential products of the action of haloperoxidase on tyrosine (Almeida et al., 2001). In contrast, Amat and Srivastava (1985; Amat 1985) reported the extraction of only iodide from *Laminaria*, not detecting iodotyrosines. All these results were obtained after heating and drying or extraction of algal tissues. Due to the chemical instability of many organic iodine compounds and the reactivity of the biological medium, they have to be taken with a certain caution, and non-invasive, *in situ* measurements like X-ray absorption spectroscopy appear desirable. Furthermore, non-invasive methods are indispensable to study functional aspects of intracellular iodine chemistry, under different physiological circumstances.

Like iodine, bromine is an essential trace element for the growth of brown (Woolery & Lewin, 1973) and red (von Stosch, 1962) macroalgae. The concentration of bromine in seawater is three orders of magnitude higher (0.7 mM, virtually all bromide ion) than that of iodine, and it is incorporated by various organisms (bacteria, diatoms, algae) in a stunning variety of organic compounds (Gribble 2000). It is imaginable that like that of iodine, the accumulation of bromine by algae is mediated by haloperoxidase, again raising the question in what form it is stored. In fact many of the volatile organohalogens formed by the algae, as mentioned above for iodine, are mixed iodine/bromine compounds (Carpenter *et al.*, 2000).

In setting up the study we were particularly interested in two aspects: i) the determination of the oxidation state from the edge, and ii) the determination of the chemical environment from the fine structure. The X-ray absorption spectrum (XAS, Koningsberger & Prins, 1988) can be divided in 2 parts, viz. the region near the edge or X-ray absorption near-edge spectrum (XANES), and the region extending a few hundreds of eV beyond the edge, the so-called extended X-ray absorption fine structure (EXAFS). As it is expected that the edge position in the XANES part of the spectrum will shift to higher energy when the charge on the central atom is higher, this gives information on its (formal) oxidation state. The

intensity of possible transitions in the edge region usually gives information on the symmetry of the environment, and the edge shape has been adequately reproduced in recent model calculations (Mijovilovich & Meyer-Klaucke, 2003; Benfatto & Della-Longa, 2001). Moreover, the white line intensity correlates for similar systems with the number of ligands, as demonstrated in as study on non-heme iron in phenylalanine hydroxylase (Mijovilovich & Meyer-Klaucke, 2003). The EXAFS part of the spectrum in fact measures X-ray induced electron diffraction, constituting an interference pattern of electron waves going out of the central atom and backscattered by surrounding atoms; it can be background subtracted and Fourier-transformed to reveal, after phase correction, a radial distribution function of atoms around the central atom.

Earlier applications of XAS to halogens in biological systems focussed on the possible coordination of halogens to metal ions, viz. of Br to V in haloperoxidase (Dau et al., 1999; Rehder et al., 2000), and of Cl to Mn in photosynthetic systems (Rompel et al., 1997). In an early application of XAS on iodine in a biological system, a study (Hashimoto & Ishii, 2000) on iodine in the strawberry conch *Strombus luhuanus* (Ishii, 1997), an environment of carbon neighbours, presumably in a protein, was identified, which was however not defined. In the case of organoiodine or –bromine compounds, it is of interest to see if there are shells in the Fourier transforms of the spectra beyond the first shell of directly bound carbon, that allow to discriminate between the incorporation of the halogen atom in a molecule that has just a single carbon, or in a molecule where the carbon is either in an aliphatic or an aromatic environment. Besides representatives of inorganic iodine (iodide, iodate) and corresponding bromine compounds, covering the range of oxidation states of -1 till to +7 for iodine, a selection of organohalogen compounds with the halogen in various biologically relevant environments were therefore measured, compared, and simulated.

It was realized that in the case of the presence of additional shells in the Fourier transforms, the spectra would have to be analysed and simulated with multiple scattering calculations. In an earlier XAS study on organobromine compounds, simulations for a similar set of compounds using the simulation programme GNXAS were reported (Burattini et al., 1993), which were in good agreement with the experimental data and described the multiple scattering phenomena adequately. The earlier aforementioned biological Br studies used the analysis programme FEFFIT (Stern et al., 1995). In the present study, we preferred the application of EXCURVE (Gurman et al., 1984, 1986, Binsted et al., 1992). Due to its

restrained refinement option it is better adapted to deal with one specific target of this study, the discrimination between aliphatic and aromatic compounds in an unknown biological sample.

Material and Methods

Compounds. 3-iodotyrosine, 3,5-diiodotyrosine, 4-bromophenylalanine, and 3,5-dibromotyrosine were from Sigma, iodoform was from Acros, all other compounds were from Aldrich.

EXAFS measurements. EXAFS measurements were carried out in the European Molecular Biology Laboratory (EMBL) Outstation in the Hamburg Synchrotron Laboratory (HASYLAB) at the Deutsches Elektronensynchrotron (DESY) in Hamburg, Germany. For I K edge measurements, a Si 311 monochromator was used and the station was set up without a focussing mirror. For Br K edge measurements the setup comprised a Si 111 monochromator and a focussing mirror with an cut-off energy of 21.5 keV. In both cases monochromators were order sorting and set at 50 % of peak intensity to suppress harmonics (Hermes *et al.*, 1984). During data collection, the storage ring DORIS III was operated at 4.5 GeV with ring currents between 150 and 90 mA. The EXAFS station features a CANBERRA 13 element solid-state fluorescence detector which was used for the solution measurements. Solid samples were diluted in BN to a concentration which would approximately give an edge step of the X-ray absorption coefficient μ of 1. HESAR glass cells with Kapton (or polyimide) windows were used for the solid samples and the aqueous solutions; for organic solvents we used a glueless cell with kapton windows (Sprakel et al., 2002). For the Br K edge measurements, the energy calibration device (Pettifer & Hermes, 1985) was applied. Scans at the I K edge were calibrated by reference to the absorption spectrum of a NaI sample between the signal ion chamber and the calibrator detector. Typically 3-5 scans per sample were taken. The sample was kept at 20 K during the measurements and moved in between scans so that the part of the sample that was exposed to the beam was varied as much as possible. No spectroscopic differences between scans were observed.

EXAFS data reduction and simulations. Data reduction was carried out at the EMBL and in Nijmegen with the EMBL Outstation data reduction package (Nolting & Hermes, 1992) including the energy calibration programmes CALIB and ROTAX, the averaging

programme AVERAGE, and the background subtraction programme REMOVE. Simulations of the calibrated, averaged, and background-subtracted EXAFS were carried out on the CLRC Daresbury Laboratory (Warrington, UK) dedicated EXAFS computer xrsserv1 and at the EMBL computer butthead using the 1998 release of the EXAFS simulation progamme EXCURVE (Gurman *et al.*, 1984, 1986; Binsted *et al.*, 1991). The *ab initio* calculation of phase shift and backscattering factors in EXCURVE was run with its default options, i.e. Hedin-Lundqvist ground state (Hedin & Lundqvist, 1969) and the von Barth exchange potential (von Barth & Hedin, 1972). Multiple scattering simulations were run in the default setting of small-atom approximation (Rehr & Albers, 1990) with the maximum path length (plmax) extended from the default value of 10 to 15 Å where appropriate. EXCURVE was selected for the EXAFS simulations because of the possibility to simulate and iteratively refine the multiple scattering of rigid ring systems with restraints (Binsted *et al.*, 1992). The difference between constrained refinement, in which an idealized geometry is imposed, and restrained refinement is that in the latter more parameters are refined but that deviations from idealized values for the interatomic distances are weighted and incorporated in the fit index during the iteration. In the present work, restrained refinements of the EXAFS of aromatic iodine and bromine compounds were run by analogy to our previous work on Cu pyridine complexes (Feiters et al., 1999).

Results and Discussion

- - - FIGURE 2, 3, CHART 1 - - -

A comparison of edges of compounds with different formal oxidation states for iodine is made in Figure 2 (see Chart 1 for structures). The energy at half-height of such edges has been found to be a reasonably reliable measure of the edge position (Dau et al., 2003). For a series of iodine compounds, we observe that the edge position shifts to higher energy with valence, going from iodine in BN (formal valence 0, 33164.1 eV) to o-iodosobenzoic acid (+1, 33165.4 eV), iodate (+5, 33167.8 eV), and periodate (+7, 33168.5 eV). However, it should be noted that iodide (formal valence -1, 33167.7 eV) does not follow the trend, having approximately the same energy at half-height as iodate (+5), and there is still a considerable energy step from periodate to H_5IO_6 (33170.3 eV) although there is no change in formal valence. The iodine and iodide spectra do not exhibit special features, but for the other compounds the intensity of the white line between 33170 and 33180 eV is found to increase

roughly with the number of oxygens bound to iodine, going from o-iodosobenzoic acid via iodate to periodate and its fully hydrated form, H_5IO_6, whereas the shoulder at 33190 eV is particularly strong in iodine compounds with a large number of doubly bound oxygens. Considering that the doubly bound oxygens are at average at shorter distance from the iodine than the other oxygens, the shift to higher energy for the edge position going from periodate to H_5IO_6 is in line with the observed shift to higher energy with longer average ligand distance for Mn compounds (Dau et al., 2003). Compared to Figure 2, the edges of the organic iodine compounds (Figure 3, see Charts 1 and 2 for structures) do not show characteristic features, and therefore do not allow distinction of the chemical speciation of iodine in these compounds, unlike the situation for e.g. sulfur compounds when measured at the sulfur K edge (George & Gorbaty, 1989; Pickering et al., 2001). The position of the edge for the organic compounds could have been expected to depend e.g. on the number of other iodine atoms bound to a carbon, or the hybridization of the carbon, but the energy resolution (±2 eV) is too low to allow these trends, if at all present, to be distinguished. Compared to the Br K edge spectra, which will be discussed below, the I K edges are relatively featureless. The difference is due to the core hole lifetime effect for iodine, i.e. the broadening of the spectral features because of the reduced lifetime of the excited state. The iodine compounds might show more characteristic features at the L edge but that was not included in this study, because i) the mean free path of photons in biological material at the energy of the I L edge (L_3 edge at 4560 eV) is relatively short, resulting in a large absorption and a low fluorescence yield compared to the I K edge, and ii) the EXAFS energy range for the I L edge is limited to 300 eV, due to the partial overlap of the three L edges.

- - - FIGURE 4, TABLE 1 - - -

The EXAFS and Fourier transform of the sodium iodate ion in aqueous solution (Figure 4b) show very strong signals, which can be simulated with a shell of close oxygens at 1.79 Å (Table 1) in line with recent literature results (Bonhoure et al., 2002). On the contrary, the weak signal observed for the sodium iodide solution (Figure 4a) reflects the absence of any atoms covalently bound to the atom of the iodide ion, the only detectable contribution being the oxygen atoms of the first shell of solvation by water molecules. The distance of 3.56 Å is in good agreement with the values of 3.60 Å found in an X-ray diffraction study on a concentrated aqueous NaI solution (Maeda & Ohtaki, 1975) and the 3.50 Å from earlier EXAFS studies (Tanida & Watanabe, 2000). The occupancy of 10 appears to be somewhat

overestimated compared to the value of 6 that was assumed in those studies, but agrees well with the 10-11 close oxygens identified in the environment of iodide ion in a X-ray crystallographic study (Thiele & Putzas, 1984).

- - - FIGURE 5, CHART 2 - - -

The EXAFS and Fourier transforms of iodine (Figure 5b) shows the effect of iodine backscattering, which can be distinguished from other backscattering contributions like that of carbon, by its characteristic higher amplitude at higher k, as also shown by the spectra of various organic compounds containing multiple iodine atoms, like iodoform (CHI_3, Figure 5a) and 1,2-diiodoethane (EtI_2, Figure 5c). In the simulations of the latter, the I-I distance is relatively close, suggesting a preferential gauche conformation of the C-C bond. The spectra of the organoiodine compounds indicate that there are contributions of other atoms than just the carbon bound to the central iodine atom; this means that unlike the I K edge spectra, the I K EXAFS would offer the possibility to distinguish different chemical environments for iodine even within the class of organoiodine compounds. It is therefore of interest to compare the spectra of aliphatic iodine compounds like that of 1,2-diiodoethane (Figure 5c) to those of aromatic compounds, for example 3-iodotyrosine (Figure 5d). Interestingly, the latter spectrum shows in its Fourier transform the pattern that is known from studies of metal complexes to be characteristic for coordination of a metal by a (hetero-)aromatic ring, such as observed for Cu pyridine complexes (Karlin et al., 1988; Feiters et al., 1999); even the atoms that would appear to be very remote from the central atom contribute very strongly to the spectrum, due to the rigidity of the ring, and the presence of reinforcing multiple scattering effects in it. Clearly, aliphatic and aromatic organoiodine compounds can be distinguished on the basis of the EXAFS spectra, in particular their Fourier transforms. This is a very important insight which is expected to have its impact on biological iodine EXAFS studies.

The simulations for the compounds containing multiple iodine atoms in Figures 5a-c and Figure 5e show that the characteristic amplitude envelope of iodine is well reproduced at various distances. The EXAFS in Figures 5a-c is dominated by the backscattering of the other iodine atoms in the molecule, which has a high amplitude at high k; this tends to suppress the significance in the refinement of weaker contributions that dominate the spectrum at lower k. This effect results in deviations between experimental and simulated spectra but according to the Fourier transforms these are due only to contributions at relatively large distances from

the central atom; hence there is no reason to question the result of the simulation for the contributions at low R in the Fourier transform. Refining in k- instead of k^3-weighting did not result in a better agreement for the low-k region of the EXAFS, as judged by visual inspection. The result for the simulation of the spectrum of elementary iodine for the iodine-iodine distance (Table 1, 2.71 Å) is in reasonable agreement with the literature value of 2.67 Å (Cotton & Wilkinson, 1988). In the simulation of the 1,2-diiodoethane, the I-I distance (3.85 Å) is relatively short, indicating that the preferential relative conformation for the iodine substituents on the C-C bond is gauche; an antiperiplanar conformation would have resulted in a much longer I-I distance (approx. 5 Å). In the simulations of iodoform (Figure 5a) and 1,2-diiodoethane (Figure 5c), the distances between the I and the sp^3-hybridized C of 2.16 and 2.18 Å (Table 1) are longer than those between the I and the sp^2-hybridized C of the aromatic rings in the I-substituted tyrosines (Figure 5d-e) which are only 2.07 Å (Chart 2); this is in line with the shorter atomic radius for sp^2-hybridized compared to sp^3-hybridized carbon. In addition to the aforementioned characteristic pattern of aromatic rings the accurate distance information derived from the EXAFS offers another approach to distinguish between incorporation of iodine in an aliphatic or an aromatic compound. The multiple scattering simulations for the aromatic compounds in Figure 7d and 7e were calculated on the basis of the geometries given in Chart 2, and refined in EXCURV98 using so-called restrained refinement (Binsted et al., 1992) with the optimum values of the distances between adjacent carbons in the phenyl ring set to 1.39 Å, and those between carbons with one carbon in between to 2.41 Å.

- - - FIGURE 6, CHART 3 - - -

The edges of the organic bromine compounds (Figure 6a, see Charts 3 and 4 for structures) exhibit much more fine structure than those of the iodine compounds, because of the shorter core hole lifetime effect for heavier elements, as mentioned above. Although the traces for the two aromatic compounds, 4-bromophenylalanine and 3,5-dibromotyrosine, resemble each other most, it is not possible to use the edge structures to classify compounds as aliphatic or aromatic on the basis of the Br edge. The edge of a 10 mM aqueous solution of sodium bromate (not shown) was found to have a very intensive (intensity approximately doubled) white line compared to that of 10 mM sodium bromide (Figure 6, bottom trace), but in spite of the higher oxidation state it was only at a marginally (< 0.5 eV) higher energy.

- - - FIGURE 7, TABLE 2 - - -

The EXAFS spectra of aqueous sodium bromide (Figure 7a) and seawater (Figure 7b) could be simulated by oxygen atoms (of solvating water molecules) at 3.33 and 3.29 Å (Table 2), respectively. Due to the large distance of these oxygen atoms to the bromine and in spite of their large number, the EXAFS signal is relatively weak compared to that of other compounds as well as to that of aqueous sodium bromate (Figure 7c) which has a strong oxygen contribution at 1.65 Å (Table 2). The bromine-oxygen distance of 3.29-3.33 Å in our simulations is significantly longer than that found in a room temperature EXAFS study (3.19 Å, Tanida et al., 1994) but in good agreement with a combined room temperature EXAFS/molecular dynamics study (3.34 Å, d'Angelo et al., 1994). The occupancy found in our refined simulations (10.7-11.1) is much higher than that found in the EXAFS/molecular dynamics study (6.7, d'Angelo et al., 1994); the value in the literature is probably more accurate in view of the adequate modelling of the asymmetry in the radial distribution of the shell of solvating oxygens derived from the molecular dynamics.

It should be noted that the sodium bromide and seawater spectra contain low-frequency contributions, visible in the EXAFS as a significant depression around k = 4-5 $Å^{-1}$, and in the Fourier transform as an apparent shell of atoms at a distance lower than the first shell of simulated oxygens, which are not included in the simulation. Such contributions have been observed before for bromine (d'Angelo et al., 1993; Burattini et al., 1993) and for other elements, like Sr (d'Angelo et al, 1997), where they have been ascribed to the presence of multi-electron excitations, like the KN_1 and $KM_{4,5}$ edge (= double electron excitation involving one 1s and 3d electron). An alternative explanation is to assume that in addition to the fine structure caused by electron backscattering off surrounding atoms, the EXAFS, an additional fine structure exists, which is caused by electron backscattering off the interatomic potential (atomic EXAFS, or AXAFS) (Rehr et al., 1995; O'Grady & Ramaker, 1998; Wende & Baberschke, 1999). In both cases the question arises why we observe the phenomenon only in the specific case of the samples with aqueous bromide. We propose that this is due to incomplete removal of the low-frequency contributions in our background subtraction procedure in the case of weak EXAFS. In other studies at the Br K edge (Dau et al., 1999) contributions at lower distance, e.g. 2 Å in the case of aqueous sodium bromide, were also observed; in this case, an explanation specific for hydrated bromide ion, viz. an assignment to hydrogen atoms (from the water molecules) was proposed (in addition to other explanations).

This is of course reasonable as the hydrogen atoms are the closest atoms in the environment of the hydrated bromide, and recently, hydrogen contributions have even been discerned in the EXAFS spectra of hydrated metal ions, where oxygens, not hydrogens, are the atoms closest to the central atom (d'Angelo et al., 2002). However, in our spectra, we were unable to simulate the low-frequency contribution with hydrogen atoms, as they did not match these shells when allowed to float in a refinement. Therefore, we prefer an explanation of the low-frequency oscillation as due to a general physical atomic absorption effect and assume that it is observed only in the hydrated bromide spectra because it could not be removed in the background subtraction due to the weakness of the EXAFS in these spectra.

- - - FIGURE 8, CHART 4 - - -

The comparison of the Fourier transforms of the organobromine compounds (Figure 8, bottom panels) reveals a distinction between aromatic and aliphatic compounds can be made for bromine, as concluded before for iodine; the patterns of shells in the Fourier transforms in Figures 8c and 8d resemble those in Figures 5d and 5e, although it is shifted to lower R (distance) because bonds with bromine are shorter than bonds with iodine. The spectrum of $CHBr_3$ (Figure 8a) can be simulated with carbon and bromine contributions at 1.92 and 3.17 Å, respectively; that of 11-bromoundecanoic acid (Figure 8b) by carbons of the alkyl tail at 1.96, 2.86, and 4.27 Å. As noted before in a study of aqueous solutions of small organobromine compounds, intermolecular effects such as interaction with solvent (d'Angelo et al, 1994) or, in our case, BN and other organobromine molecules can affect the spectra; simulations of these effects fall outside the scope of the present study but this neglect does result in significant differences between the experimental spectra and fits based only on considerations of intramolecular effects. The spectrum of 4-bromophenylalanine (Figure 8c) is simulated by a contribution of a phenyl ring and an additional carbon (Chart 4, left, including multiple scattering), and that of dibromotyrosine (Figure 8d) by a phenyl ring with the second bromine at 5.65 Å as well as contributions from the oxygen of the hydroxyl group in the ring and the first carbon of the side chain (Chart 4, right, including multiple scattering. Although the difference in bond length between bonds of bromine with sp^3- or sp^2-hybridized carbon is not as large (1.92-1.96 vs. 1.87-1.88 Å) as that found for iodine, it is large enough to give significant differences in the EXAFS, thus providing an additional feature to distinguish bromine in aliphatic and aromatic environments.

Conclusions

We conclude that the iodine K edge positions and structures are sensitive to formal valence, showing an edge shift to higher energy except for iodide. The multiple scattering effects in the aromatic rings of aromatic organohalogen compounds are adequately reproduced with the restrained refinement simulations in EXCURVE. EXAFS spectra of organohalogen compounds (both iodine and bromine) can be used to discriminate between aliphatic and aromatic compounds. There are differences both in the distances from the halogens to the first shell of carbons, which are shorter for aromatic compounds, as well as in the patterns of shells in the Fourier transforms. This result is expected to be relevant to studies at these edges in biological systems.

Acknowledgements

The authors received support from the European Community in the framework of the Access to Research Infrastructure Action of the Improving Human Potential Programme to the EMBL Hamburg Outstation, contract number HPRI-CT-1999-00017. We are grateful to Peter M.H. Kroneck (Universität Konstanz) and Alison Butler (University of Santa Barbara) for stimulating and useful discussions, and for funding part of the position of FCK (through grants from the Deutsche Forschungsgemeinschaft to P.M.H. Kroneck and from the National Institutes of Health to A. Butler).

Tables

Table 1. Parameters for the simulations of the EXAFS of iodine compounds. [a)]
Energies in eV, distances in Å,
(Debye-Waller type factors quoted as $2\sigma^2$ in $Å^2$ in parentheses)

\ Sample Parameter	NaI (aq.) Fig. 4a	$NaIO_3$ (aq.) Fig. 4b	CHI_3/BN Fig. 5a	I_2/ethanol Fig. 5b	EtI_2/BN Fig. 5c
ΔEF (eV)	-5.16	-7.55	-10.66	-11.24	-3.711
Energy range @eV@	20-350	13-976	5-1166	5-1160	5-647
O	10.0 at 3.56 (0.034)	3.4 at 1.79 (0.004)	-	-	-
C	-	-	0.7 at 2.16 (0.001)	-	1.0 at 2.18 (0.005)
C	-	-	-	-	0.7 at 2.99 (0.006)
I	-	-	2.6 at 3.57 (0.005)	0.8 at 2.71 (0.004)	1.0 at 3.85 (0.006)
fit index (k^3-weighting)	2.6948	1.3019	0.6964	1.2472	1.1285

[a)] The parameters for the simulations of the aromatic iodine compounds are in Chart 2.

Table 2. Parameters for the simulations of EXAFS of bromine compounds.[a)]
Energies in eV, distances in Å,
(Debye-Waller type factors quoted as $2\sigma^2$ in $Å^2$ in parentheses)

\ Sample Parameters	NaBr (aq.) Fig.7a	Seawater Fig.7b	$NaBrO_3$ (aq.) Fig.7c	$CHBr_3$ (aq.) Fig. 8a	11-Br-undeca-noic acid/BN Fig. 8b [b)]
ΔEF (eV)	-3.25	-0.82	-9.29	-3.24	-6.37
Energy range (eV)	3-450	3-450	4-817	4-815	4-620
O	10.7 at 3.33 (0.032)	11.1 at 3.29 (0.034)	2.7 at 1.65 (0.006)	-	-
C	-	-	-	1.0 at 1.92 (0.005)	1.3 at 1.96 (0.003)
C	-	-	-	-	2.86 (0.007)
Br	-	-	-	2.9 at 3.17 (0.009)	-
C	-	-	-	-	4.27 (0.007)
fit index (k^3-weighting)	0.3790	0.4769	0.2266	0.9013	0.1900

[a)] The parameters for the simulations of the aromatic bromine compounds are in Chart 4.
[b)] All the atoms included in the simulation of 11-bromoundecanoic acid are part of a single multiple scattering unit; the occupancies for the remote shells are the same as given for the carbon attached to the central bromine

Figure captions

Chart 1. Structures of iodine compounds.

Chart 2. Structures of (left) 3-iodotyrosine (left) and 3,5-diiodotyrosine (right) with parameters of the refined simulations of Fig. 5d and 5e, respectively; all atoms were included in a multiple scattering units whose occupancies refined to 1.2 and 1.0, respectively. Distances in Å, Debye-Waller type factors quoted as $2\sigma^2$ in $Å^2$ in parentheses.
3-iodotyrosine: energy range, 18-600 eV; ΔEF, -4.137 eV; fit index (k^3-weighting), 0.1785.
(right) 3,5-diiodotyrosine: energy range, 18-600 eV; ΔEF, -0.367 eV; fit index (k^3-weighting), 0.1718.
Distances in Å, Debye-Waller type factors quoted as $2\sigma^2$ in $Å^2$ in parentheses.

Chart 3. Structures of bromine compounds.

Chart 4. Structures of 4-bromophenylalanine (left) and 3,5-dibromotyrosine (right) with parameters of the refined simulations of Fig. 7c and 7d, respectively; all atoms were included in a multiple scattering units whose occupancies refined to 1.0 for both spectra. Distances in Å, Debye-Waller type factors quoted as $2\sigma^2$ in $Å^2$ in parentheses.
4-bromophenylalanine: energy range, 25-635 eV; ΔEF, -2.162 eV; fit index (k^3-weighting), 0.1324.
3,5-dibromotyrosine: energy range, 25-635 eV; ΔEF, -3.186 eV; fit index (k^3-weighting), 0.1981.

Figure 1. Simplified biogeochemical cycle of iodine. In seawater, iodine (total conc. 0.5 mM) is mainly present as iodate, yet up to 50 % of this can be converted to iodide in the euphotic zone, presumably as a side reaction of nitrate reductase of planktonic algae and bacteria (e.g. Farrenkopf et al., 1997; Wong et al., 2002). Iodide can be taken up, possibly by the action of vanadium-containing haloperoxidase (Wever et al., 1991), by a variety of algae (Küpper et al., 1998), which constitute the major biogeochemical pump of iodine from the ocean to the atmosphere, in the form of iodinated halocarbons (Carpenter et al., 2000). Besides emission by algae, a non-biological pathway to methyl iodide formation has been suggested, based in the reaction of organic matter in seawater with I_2 or HOI formed by oxidation of I^- in the upper water column (for review: Luther et al., 1995). Iodocarbons are rapidly photolyzed and

oxidized, resulting in the formation of iodine oxide (Alicke et al., 1999). IO has recently been recognized as a contributor of condensation nuclei for cloud formation in the coastal atmosphere (O'Dowd et al., 2002), resulting in its deposition by precipitation. On land, iodine is accumulated by both terrestrial plants and animals, being an essential trace element for the biosynthesis of the thyroid hormone, thyroxin, by the action of lactoperoxidase. Part of the iodine entering the agricultural and human food chain nowadays originates from sea foods, incl. seaweeds, and from iodine supplements added to table salt from fossil iodide / iodate deposits.

Figure 2. Iodine X-ray absorption K edges of compounds (see Chart 1) of different valency of iodine, from top to bottom: NaI (20 mM in water, valency -1); I_2 (with BN, 0); o-IO-benzoic acid (+1); $NaIO_3$ (10 mM in water, +5); $NaIO_4$ (with BN, +7); H_5IO_6 (with BN, +7).

Figure 3. Iodine X-ray absorption K edges of organoiodine compounds (see Charts 1 and 2) compared with elementary iodine, from top to bottom: 1,2-diiodoethane in BN; CHI_3 in BN; I_2 in tetrahydrofuran/acetonitrile 1/1; 3-iodotyrosine; 3,5-diiodotyrosine.

Figure 4. Experimental (solid) and simulated (dashed) k^3-weighted EXAFS (top) and phase-corrected Fourier transform (bottom) of a) 20 mM NaI in water, and b) 10 mM $NaIO_3$ in water. The parameters of the simulations are listed in Table 1.

Figure 5. Experimental (solid) and simulated (dashed) k^3-weighted EXAFS (top) and phase-corrected Fourier transform (bottom) of a) CHI_3/BN, b) I_2 in tetrahydrofuran/acetonitrile 1/1, c) 1,2-diiodoethane/BN, d) 3-iodotyrosine, and e) 3,5-diiodotyrosine/BN. The parameters of the simulations in Figs. 5a, b, and c are listed in Table 1, those for Figs. 5d and 5e in Chart 2.

Figure 6. X-ray absorption K edges of bromine (see Charts 3 and 4 for structures) in (top to bottom) bromoform ($CHBr_3$); 11-Br-undecanoic acid; 4-Br-phenylalanine; 3,5-dibromotyrosine; NaBr (10 mM in water).

Figure 7. Experimental (solid) and simulated (dashed) k^3-weighted EXAFS (top) and phase-corrected Fourier transform (bottom) of a) 10 mM NaBr in water, b) Br in seawater, and c) 10 mM $NaBrO_3$ in water. The parameters of the simulations are listed in Table 2.

Figure 8. Experimental (solid) and simulated (dashed) k^3-weighted EXAFS (top) and phase-corrected Fourier transform (bottom) of a) $CHBr_3$ (aq.), b) 11-bromoundecanoic acid/BN, c) 4-bromophenylalanine/BN, and d) 3,5-dibromotyrosine/BN. The parameters of the simulations in Figs. 8a and 8b are listed in Table 2, those for Figs. 8c and 8d in Chart 4.

References

Alicke, B., Hebestreit, K., Stiutz, J. & Platt, U. (1999) *Nature* **397**, 572-573.

Almeida, M., Duarte, C., Alexandre, A., Humanes, M. & Fraústo da Silva, J. J. R. (2001) *J. Inorg. Biochem.* **86**, 121.

Amat, M. A. & Srivastava, L. M. (1985) *J. Phycol.* **21**, 330-333.

Amat, M. A. (1985) Doct. Thesis, Univ. Pierre et Marie Curie, Paris, France

Benfatto, M. & Della Longa, S. (2001) *J. Synchr. Rad.* **8**, 1087-1094.

Binsted, N., Campbell, J. W., Gurman, S. J. & Stephenson, P. C. (1991) EXCURV92, SERC Daresbury Laboratory.

Binsted, N., Strange, R. W. & Hasnain, S. S. (1992) *Biochemistry* **31**, 12117-12125.

Bonhoure, I., Scheidegger, A. M., Wieland, E. & Dähn, R. (2002) *Radiochim. Acta* **90**, 674-651.

Burattini, E., D'Angelo, P., DiCicco, A., Filipponi, A. & Pavel, N. V. (1993) *J. Phys. Chem.* **97**, 5486-5494.

Butler, A.; Carter, J. N.; Simpson, M. T. (2001) Vanadium in Proteins and Enzymes. In *Handbook on Metalloproteins*, Bertini, I., Sigel, A., Sigel, H., Eds.; Marcel Dekker: New York.

Carpenter, L. J., Malin, G., Liss, P. S., Küpper, F. C. (2000) *Global Biogeochem. Cycles* **14**, 1191-1204.

Cotton, F. A. & Wilkinson, G. *Advanced Inorganic Chemistry*, 5th Ed. Wiley-Interscience, New York, 1988.

Courtois, B. (1813) *Ann. Chim. Phys.* **88**, 311-318.

Cramer, S. P. (1988) in 'X-ray Absorption Spectroscopy' (Koningsberger, D. C. & Prins, R., editors) Wiley, New York, pp. 257-320

D'Angelo, P., Barone, V., Chillieni, G., Sanna, N., Meyer-Klaucke, W. & Pavel, N. V. (2002) *J. Am. Chem. Soc.* **124**, 1958-1967.

D'Angelo, P., Di Cicco, A., Filipponi, A. & Pavel, N. V. (1993) *Phys. Rev. A* **47**, 2055-2063.

D'Angelo, P., Di Nola, A., Filipponi, A., Pavel, N. V. & Roccatano, D. (1994) *J. Chem. Phys.* **100**, 985-994.

D'Angelo, P., Nolting, H.-F. & Pavel, N. V. (1997) *Phys. Rev. A* **53**, 798-805.

Dau, H., Dittmer, J., Epple, M., Hanss, J., Kiss, E., Rehder, D., Schulzke, C. & Vilter, H. (1999) *FEBS Lett.* **457**, 237-240.

Dau, H., Liebisch, P. & Haumann, M. (2003) *Anal. Bioanal. Chem.* **376**, 562-583.

Eschle (1897) *Z. Physiol. Chem.* **23**, 30-7

Farrenkopf, A.M., Dollhopf, M.E., Ni Chadhain, S., Luther III, G.W. & Nealson, K.H. (1997) *Mar. Chem.* **57**, 347-54

Feiters, M. C., Klein Gebbink, R. J. M., Solé, V. A., Nolting, H.-F., Karlin, K. D. & Nolte, R. J. M. (1999) *Inorg. Chem.* **38**, 6170-6180.

George, G. N. & Gorbaty, M. L. (1993) *J. Am. Chem. Soc.* **111**, 3182-3186.

Greegor, R. B., Pingitore Jr., N. E. & Lytle, F. W. (1997) *Science* **275**, 1452-1454.

Gribble, G. W. (2000) *Environ. Sci. & Polut. Res.* **7**, 37-49.

Gurman, S. J., Binsted, N. & Ross, I. (1984) *J. Phys. C., Solid State Phys.* **17**, 143-151.

Gurman, S. J., Binsted, N. & Ross, I. (1986) *J. Phys. C., Solid State Phys.* **19**, 1845-1861.

Harris, H.H., Pickering, I.J., George, G.N. (2003) *Science* **301**, 1203.

Hashimoto, H. & Ishii, T. (2000) *Proc. 11th Int. Conf. on X-Ray Absorption Fine Structure*, Ako, Japan, p. 258.

Hedin, L. & Lundqvist, S. (1969) in: Seitz, F., Turnbull, D., Ehrenreich, H. (Eds.) *Solid State Physics*, vol. 23, Academic Press, New York, pp. 2-181.

Hermes, C., Gilberg, E. & Koch, M. H. J. (1984) *Nucl. Instrum. & Methods* **222**, 207-214.

Ishii, T. (1997) *Fisheries Science* **63**, 646-647.

Karlin, K. D., Ghosh, P., Cruse, R. W., Farooq, A., Gultneh, Y., Jacobsen, R. R., Blackburn, N. J., Strange, R. W. & Zubieta, J. (1988) *J. Am. Chem. Soc.* **110**, 6769-6780.

Koningsberger, D. C. & Prins, R., Eds. (1988) *X-ray Absorption*, Wiley Interscience, New York

Küpper, F. C., Schweigert, N., ArGall, E., Legendre, J. M., Vilter, H. & Kloareg, B. (1998) *Planta* **207**, 163-171.

Kylin, H, (1929) *Hoppe-Seyler's Z. Physiol. Chem.* **186**, 50-84.

Lee, A., Lin, Z.-Q., Pickering, I. J. & Terry, N. (2001) *Planta* **213**, 977-980.

Luther III, G. W. Wu, J. & Cullen, J. B. (1995) *Adv. Chem. Ser.* **244**, 135-155.

Maeda, M. & Ohtaki, H. (1975) *Bull. Chem. Soc. Jpn.* **48**, 3755-3756.

Mijovilovich, A. & Meyer-Klaucke, W. (2003) *J. Synchrotron Rad.* **10**, 64-69.

Nolting, H.-F. & Hermes, C. (1992) EXPROG Exafs data reduction package, EMBL Outstation Hamburg, Germany.

O'Dowd, C. D., Jimenez, J. L., Bahrein, R., Flagan, R. C., Seinfeld, J. H., Hämeri, K., Pirjola, L., Kulmala, M., Jennings, S. G. & Hoffmann, T. (2002) *Nature* **417**, 632-636.

O'Grady, W. E. & Ramaker, D. E. (1998) *Electrochimica Acta* **44**, 1283-1287.

Pettifer, R. F. & Hermes, C. (1985) *J. Appl. Crystallogr.* **18**, 404-412.

Pickering, I. J., George, G. N., van Fleet-Stalder, V., Chasteen, T. G. & Prince, R. C. (1999) *J. Biol. Inorg. Chem.* **4**, 791-794.

Pickering, I. J., George, G. N., Yu, E. Y., Brune, D. C., Tuschak, C., Overmann, J., Beatty, J. T., Prince, R. C. (2001) *Biochemistry* **40**, 8138-8145.

Pickering, I. J., Prince, R. C., Divers, T. & George, G. N. (1998) *FEBS Lett.* **441**, 11-14.

Rehder, D., Schulzke, C., Dau, H., Meinke, C., Hanss, J. & Epple, M. (2000) *J. Inorg. Biochem.* **80**, 115-121.

Rehr, J. J. & Albers, R. C. (1990) *Phys. Rev. B.* **41**, 8139-8149.

Rehr, J. J., Zabinsky, S. I., Ankudinov, A. & Albers, R. C. (1995) *Physica B.* **208-209**, 23-26.

Roche, J. & Yagi, Y. (1952) *C. R. Soc. Biol. Paris* **146**, 642-645.

Rompel, A., Andrews, J. C., Cinco, R. M., Wemple, M. W., Christou, G., Law, N. A., Pecoraro, V. L., Sauer, K., Yachandra, V. K. & Klein, M. P. (1997) *J. Am. Chem. Soc.* **119**, 4465-4470.

Sprakel, V. S. I., Feiters, M. C., Nolte, R. J. M., Hombergen, P. M. F. M., Groenen, A., de Haas, H. J. R. (2002) *Rev. Sci. Instrum.* **73**, 2994-2998.

Stern, E. A., Newville, M., Ravel, B., Yacoby, Y. & Haskel, D. (1995) *Physica B* **117**, 208-209.

Tanida, H., Sakane, H. & Watanabe, I. (1994) *J. Chem. Soc. Dalton Trans.* 2321-2326

Tanida, H. & Watanabe, I. (2000) *Bull. Chem. Soc. Jpn.* **73**, 2747-2752.

Thiele, G. & Putzas, D (1984) Z. Anorg. Allg. Chem. **519**, 217-224.

Von Barth, U. & Hedin, L. (1972) *J. Phys. C* **5**, 1629-1642.

von Stosch, H. A. (1962) *Naturwissenschaften* **49**, 42-3.

Wende, H. & Baberschke, K. (1999) *J. Electron Spectr. Relat. Phenom.* **101-103**, 821-826.

Wong, G. T. F., Piumsomboon, A. U., Dunstan, W. M. (2002) *Mar. Ecol. Prog. Ser.* **237**, 27-39.

Woolery, M. L., Lewin, R. A. (1973) *Phycologia* **12**, 131-8.

Figures

Chart 1

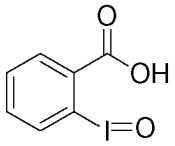

o-iodosobenzoic acid

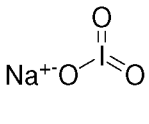

$NaIO_3$

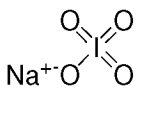

$NaIO_4$

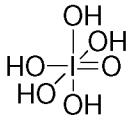

H_5IO_6

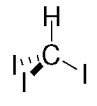

iodoform

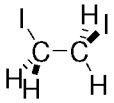

(gauche) 1,2-diiodoethane *(anti)*

Chart 2

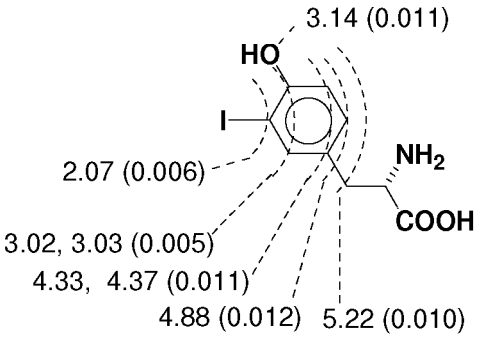

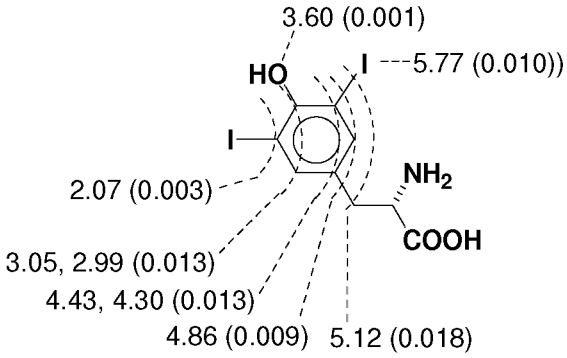

Chart 3

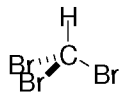

bromoform

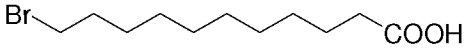

11-bromoundecanoic acid

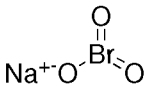

$NaBrO_3$

Chart 4

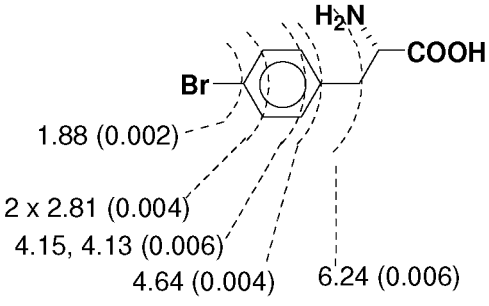

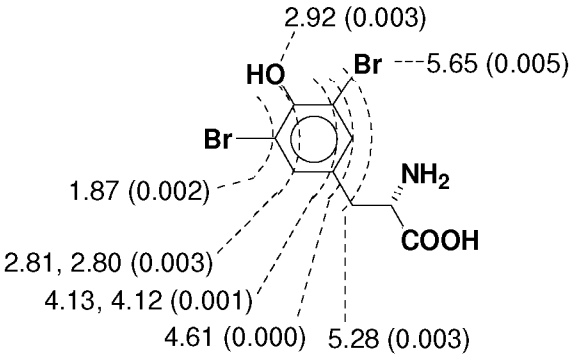

Figure 1

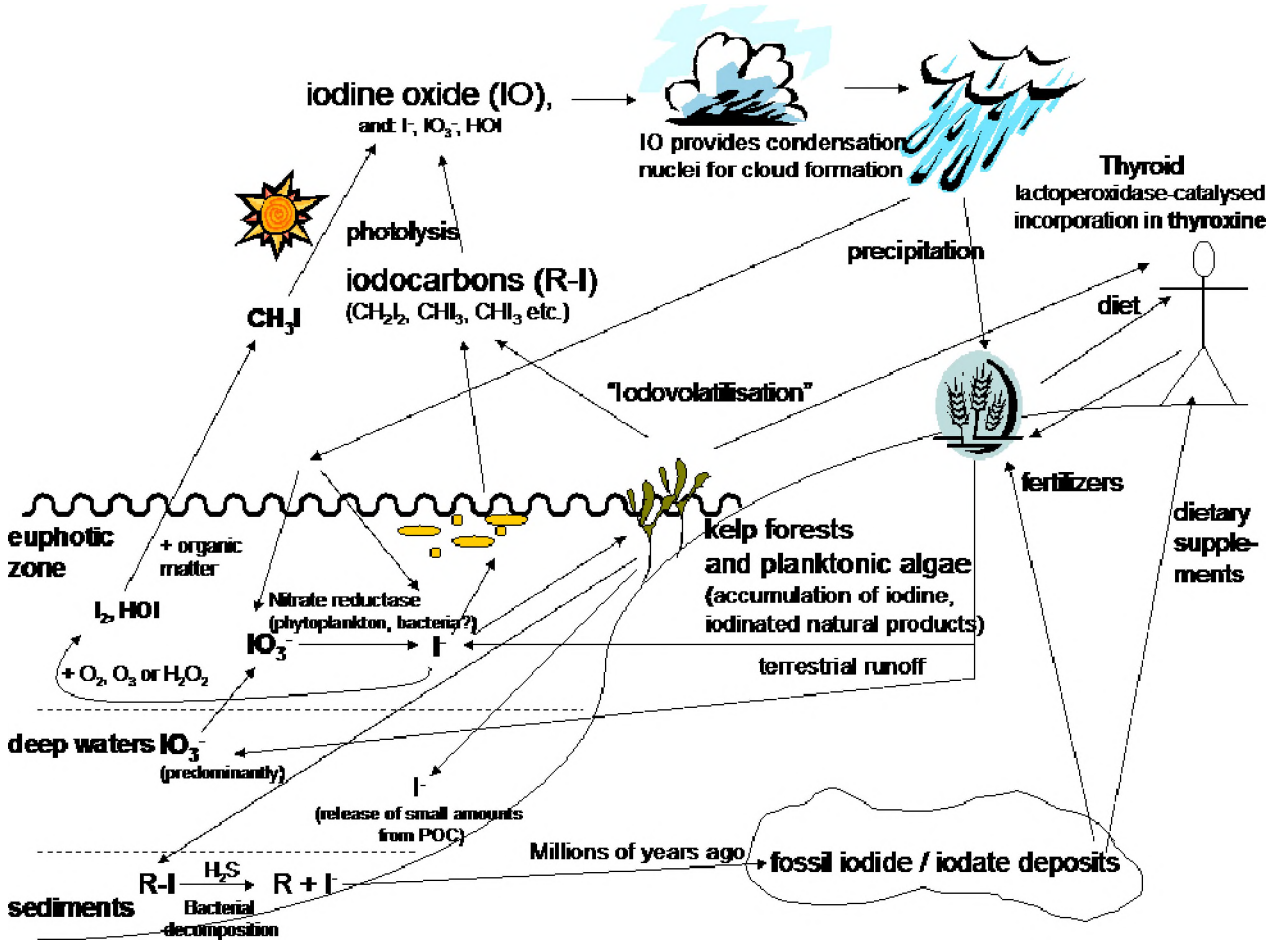
iodine oxide (IO),
and: I-, IO3-, HOI
IO provides condensation nuclei for cloud formation
Thyroid
lactoperoxidase-catalysed incorporation in thyroxine
photolysis
iodocarbons (R-I)
(CH2I2, CHI3, C2HI3 etc.)
CH3I
precipitation
diet
"Iodovolatilisation"
fertilizers
dietary supple-ments
euphotic zone
+ organic matter
I2, HOI
Nitrate reductase (phytoplankton, bacteria?)
IO3- → I-
+ O2, O3 or H2O2
kelp forests and planktonic algae
(accumulation of iodine, iodinated natural products)
terrestrial runoff
deep waters IO3-
(predominantly)
I-
(release of small amounts from POC)
Millions of years ago
fossil iodide / iodate deposits
sediments
R-I → (H2S, Bacterial decomposition) R + I-

Figure 2

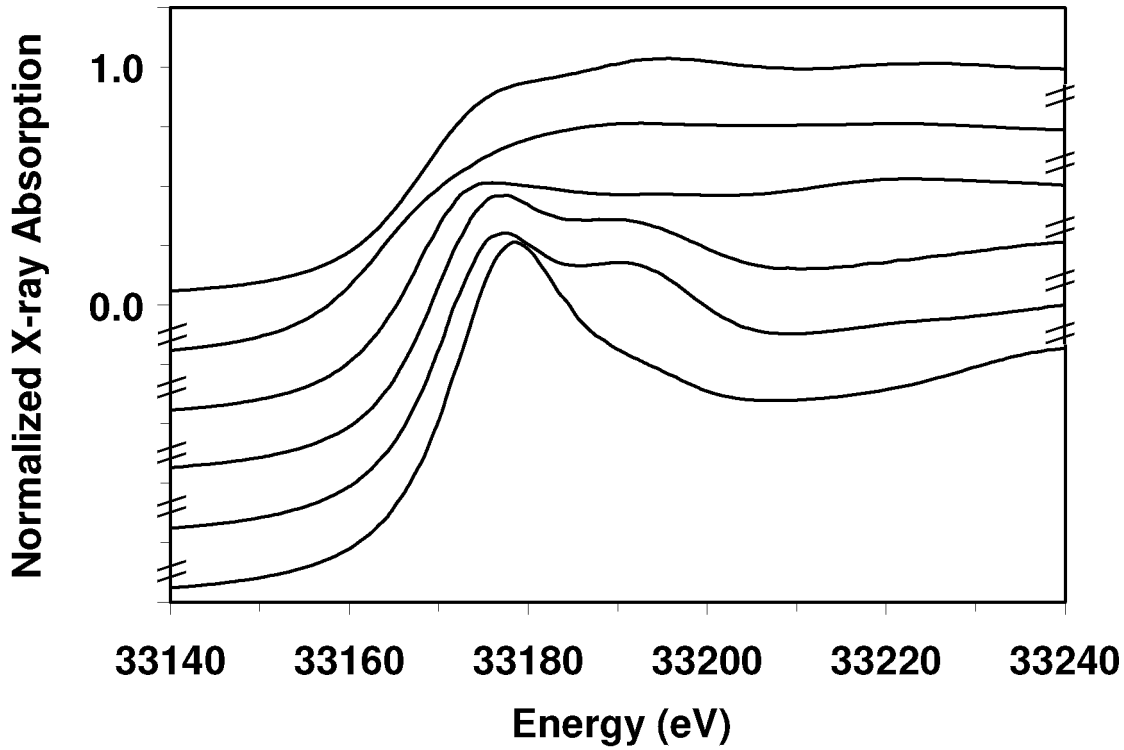
Normalized X-ray Absorption
1.0
0.0
33140
33160
33180
33200
33220
33240
Energy (eV)

Figure 3

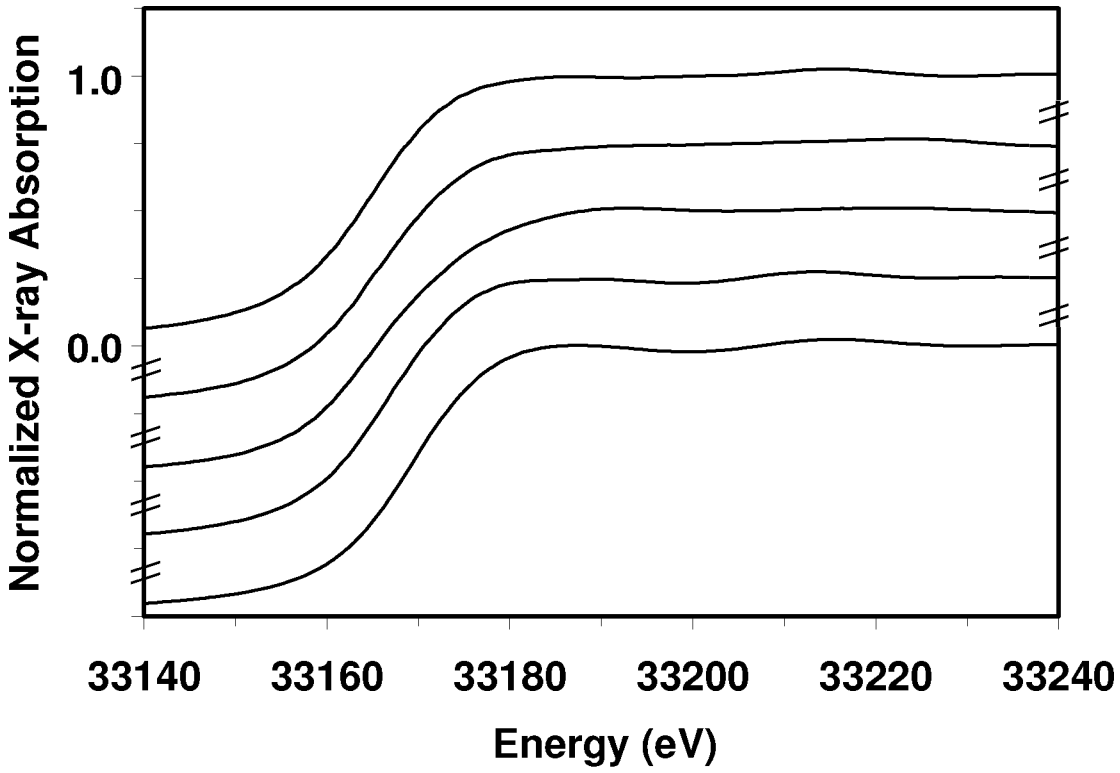
Normalized X-ray Absorption
1.0
0.0
33140
33160
33180
33200
33220
33240
Energy (eV)

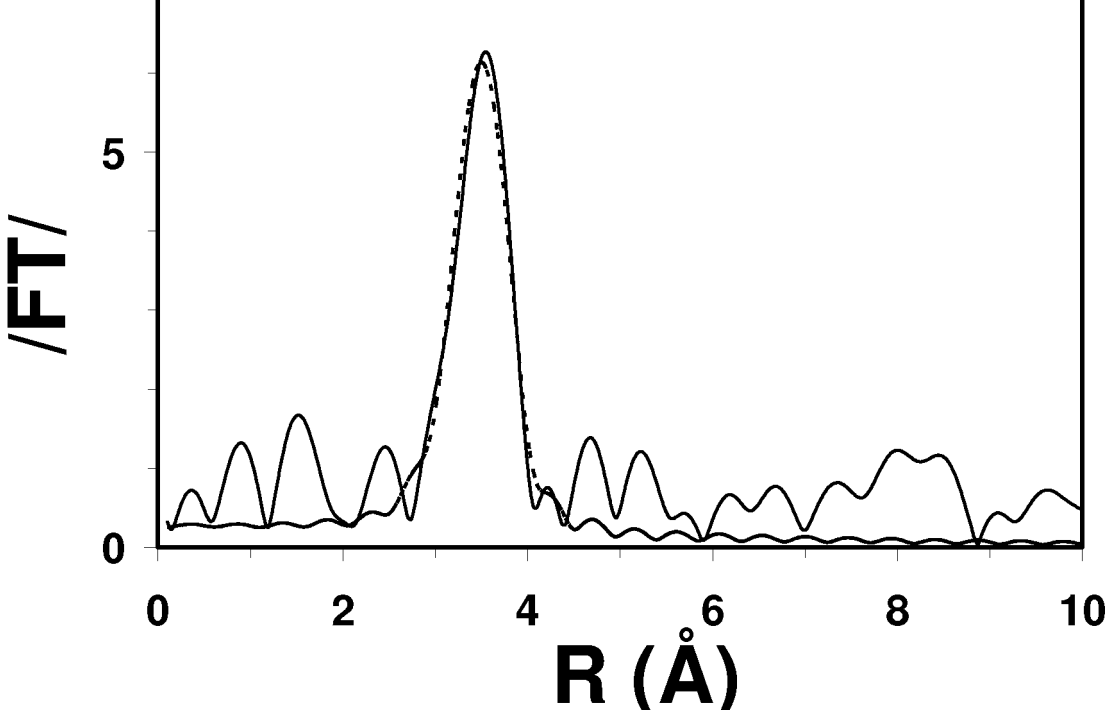
/FT/
5
0
0
2
4
6
8
10
R (Å)

Figure 4a

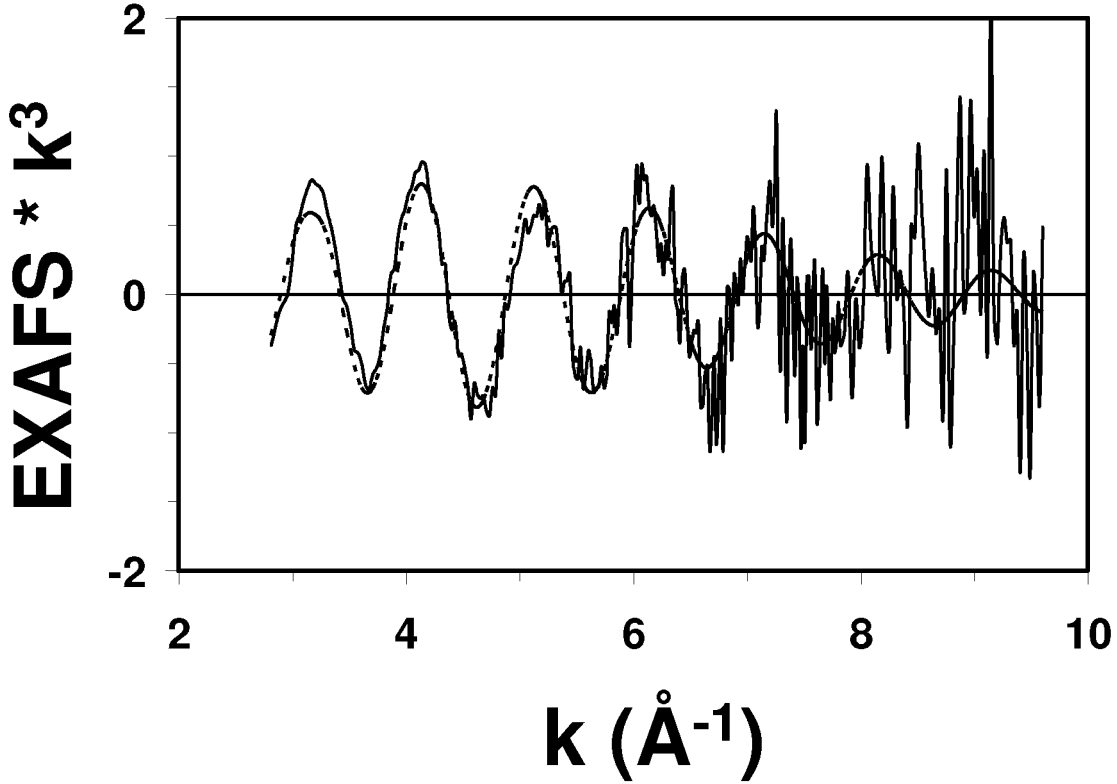

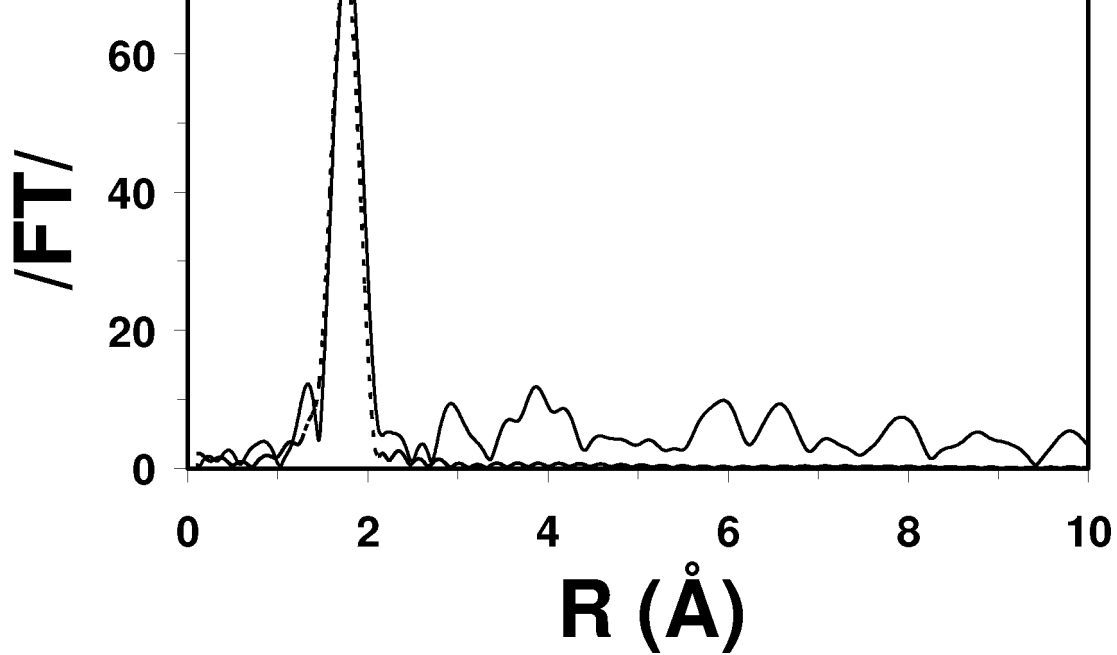
/FT/
60
40
20
0
0
2
4
6
8
10
R (Å)

Figure 4b

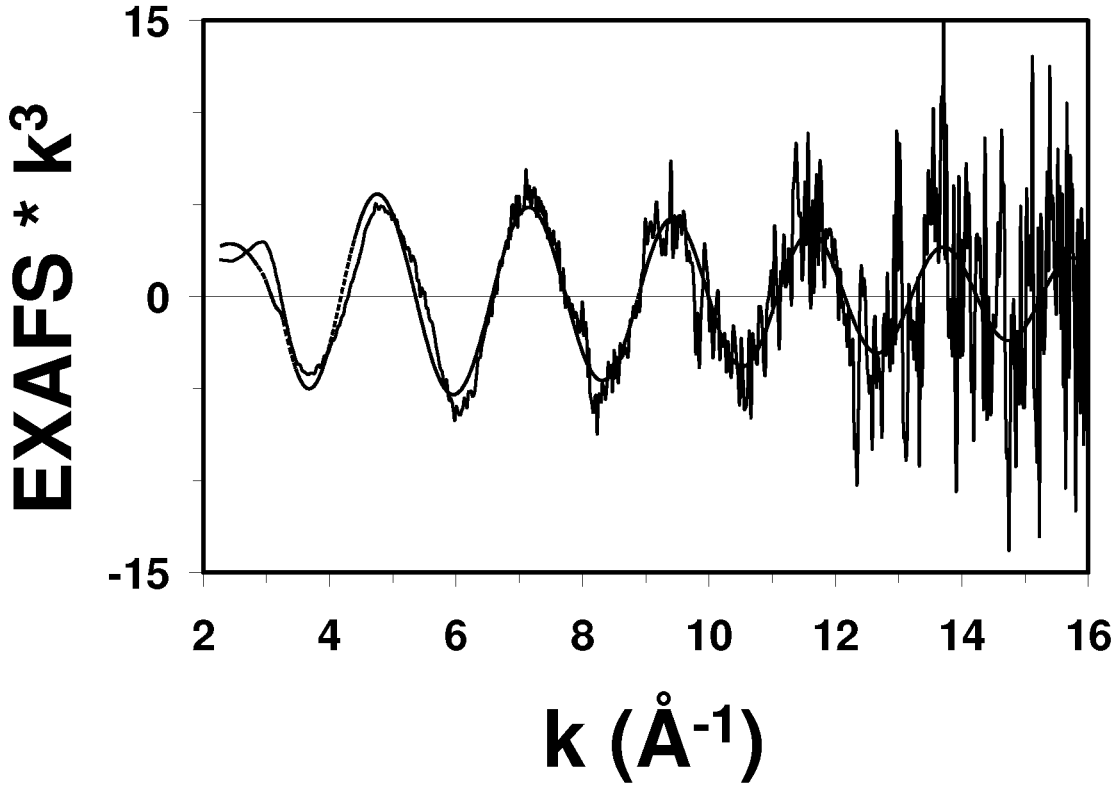

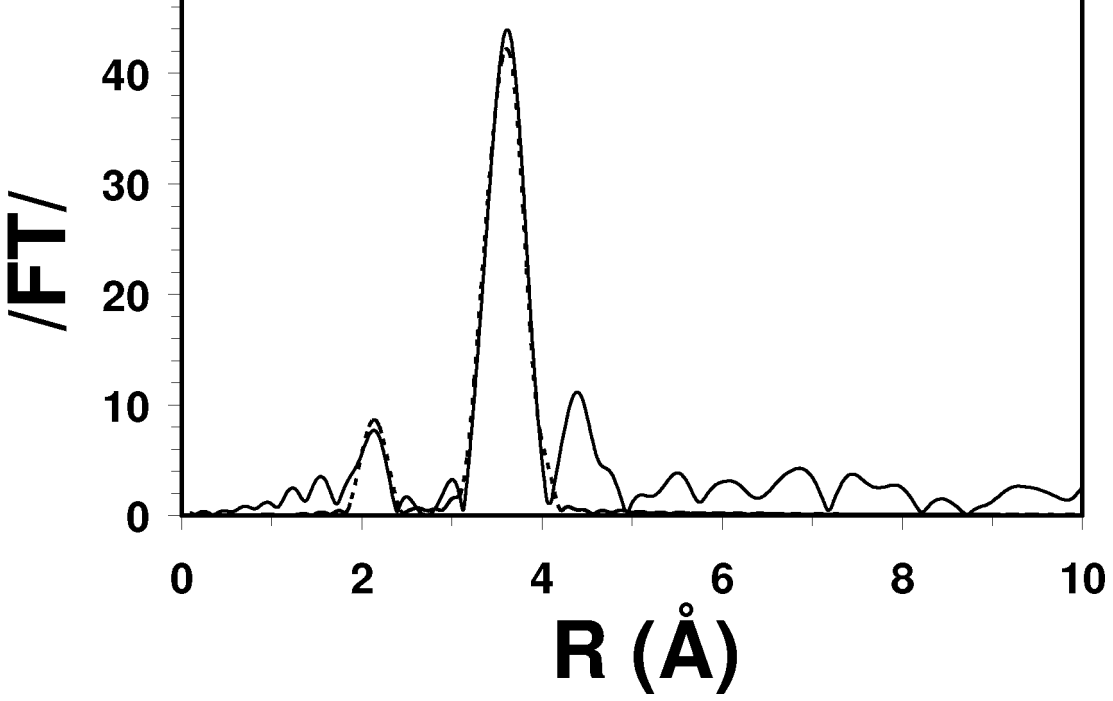
/FT/
40
30
20
10
0
0
2
4
6
8
10
R (Å)

Figure 5a

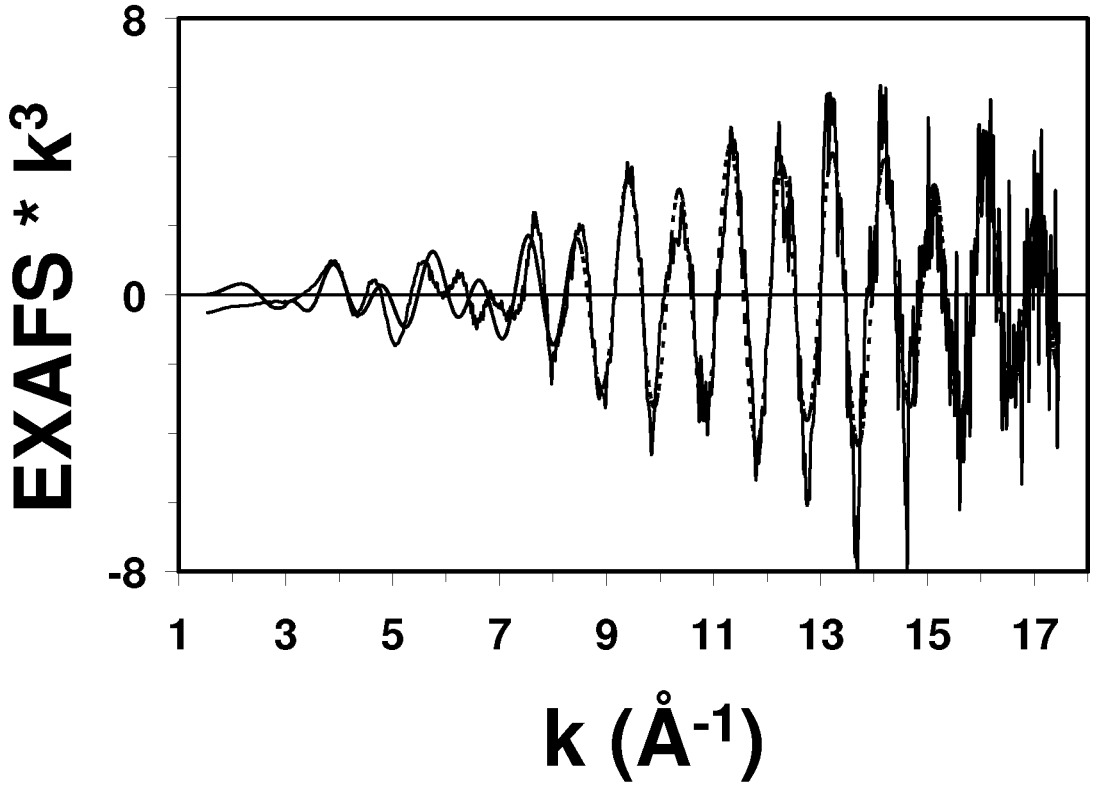

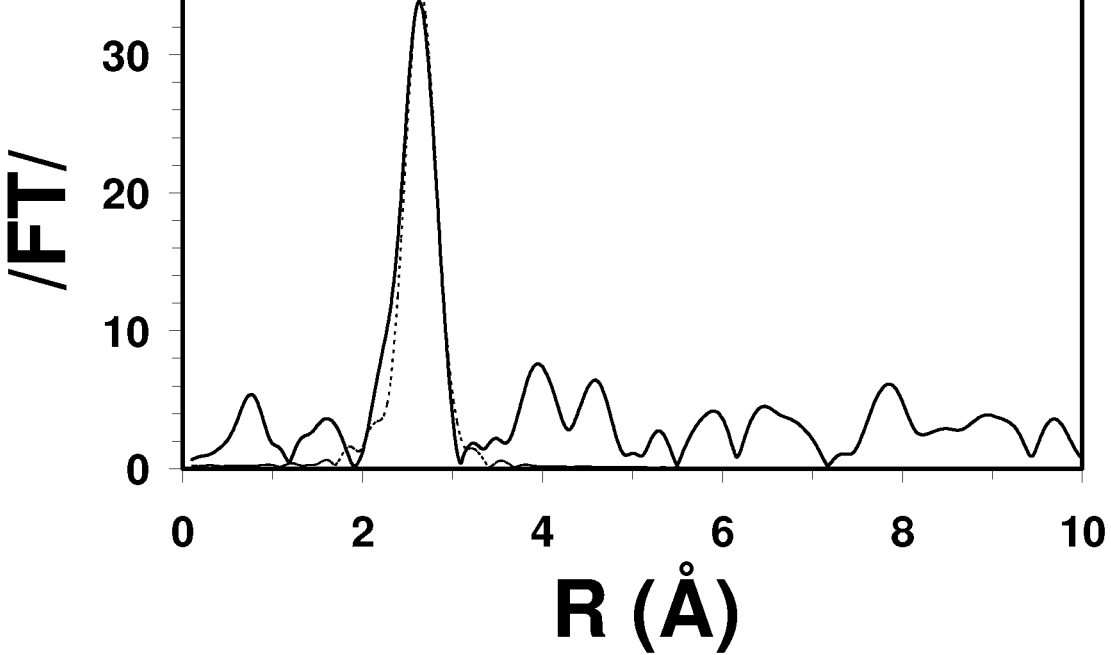
/FT/
30
20
10
0
0
2
4
6
8
10
R (Å)

Figure 5b

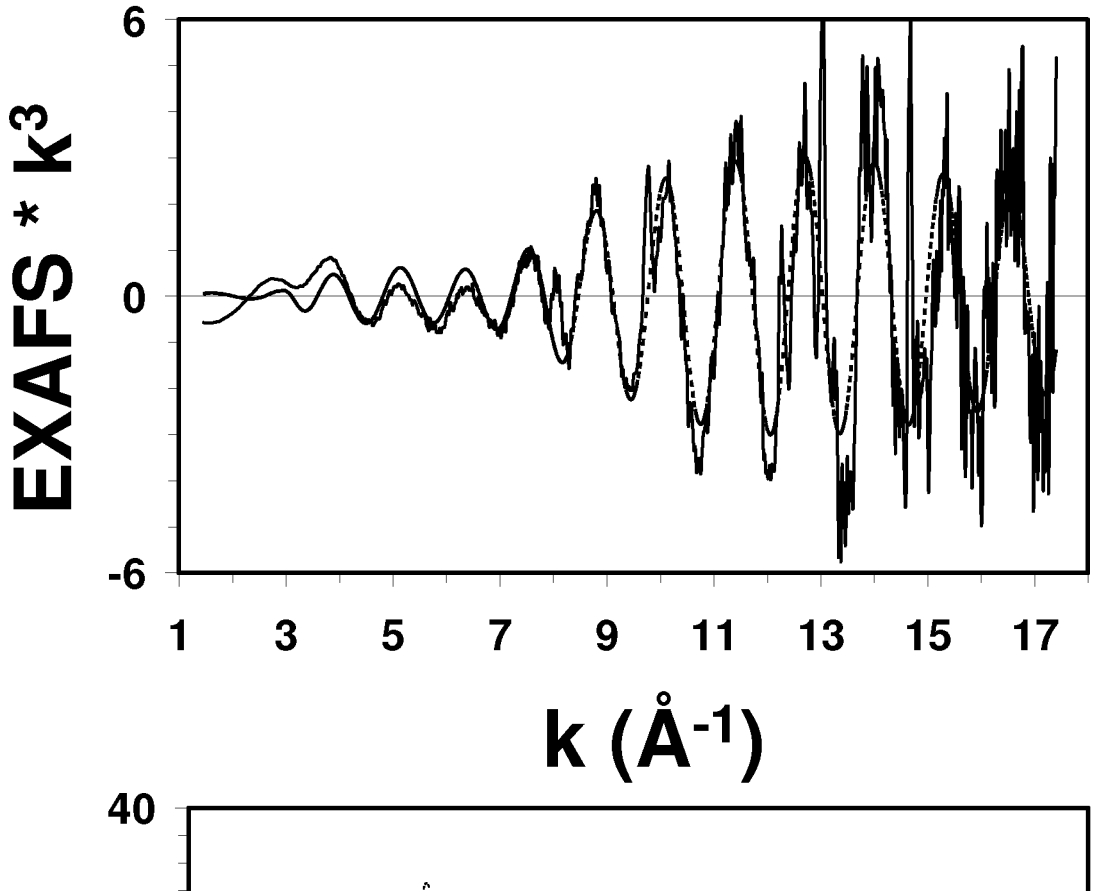

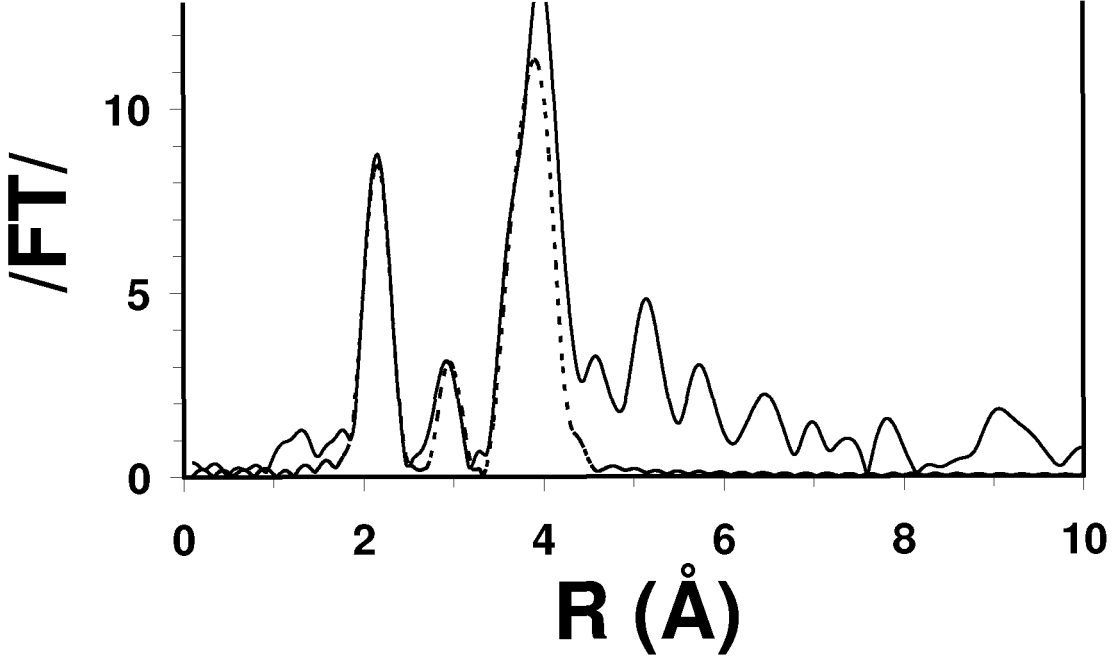
/FT/
10
5
0
0
2
4
6
8
10
R (Å)

Figure 5c

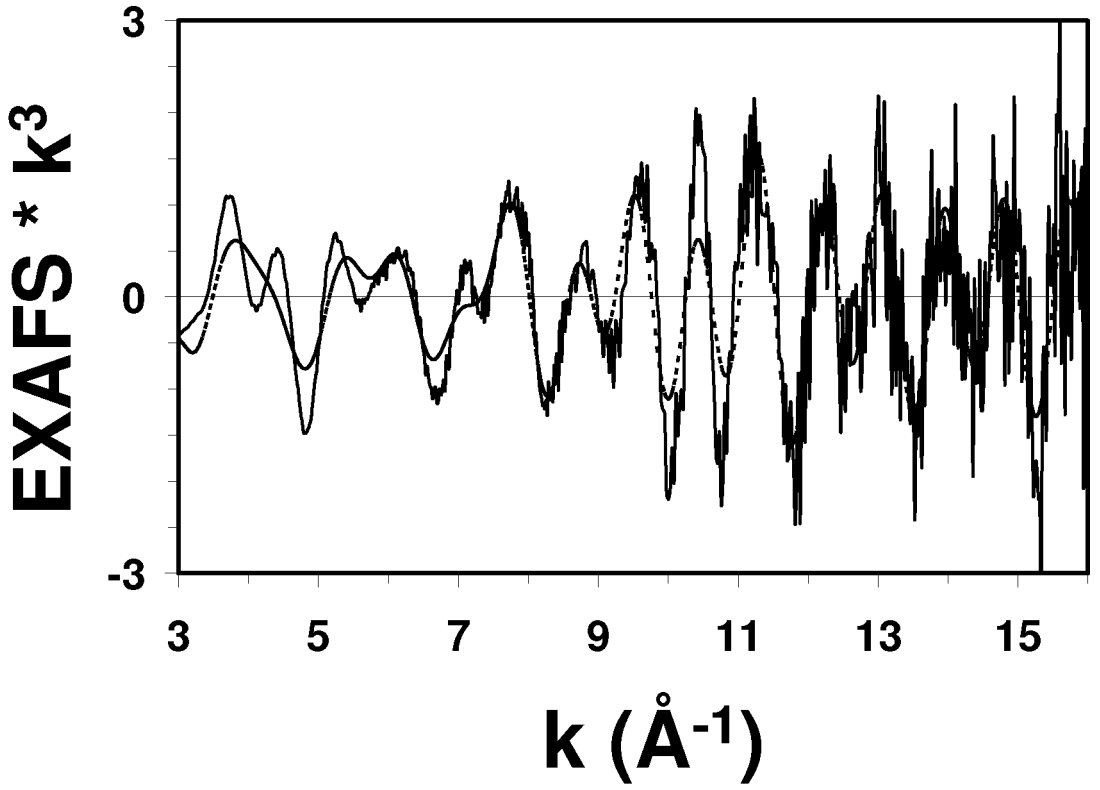

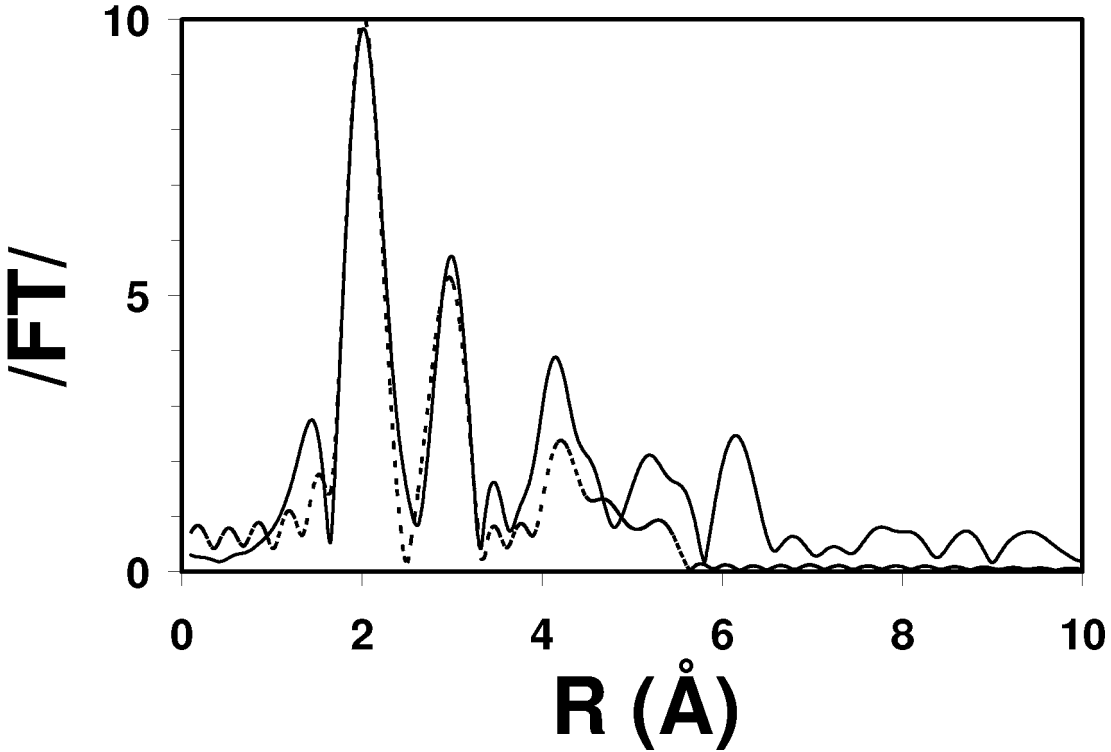
10
5
0
/FT/
0
2
4
6
8
10
R (Å)

Figure 5d

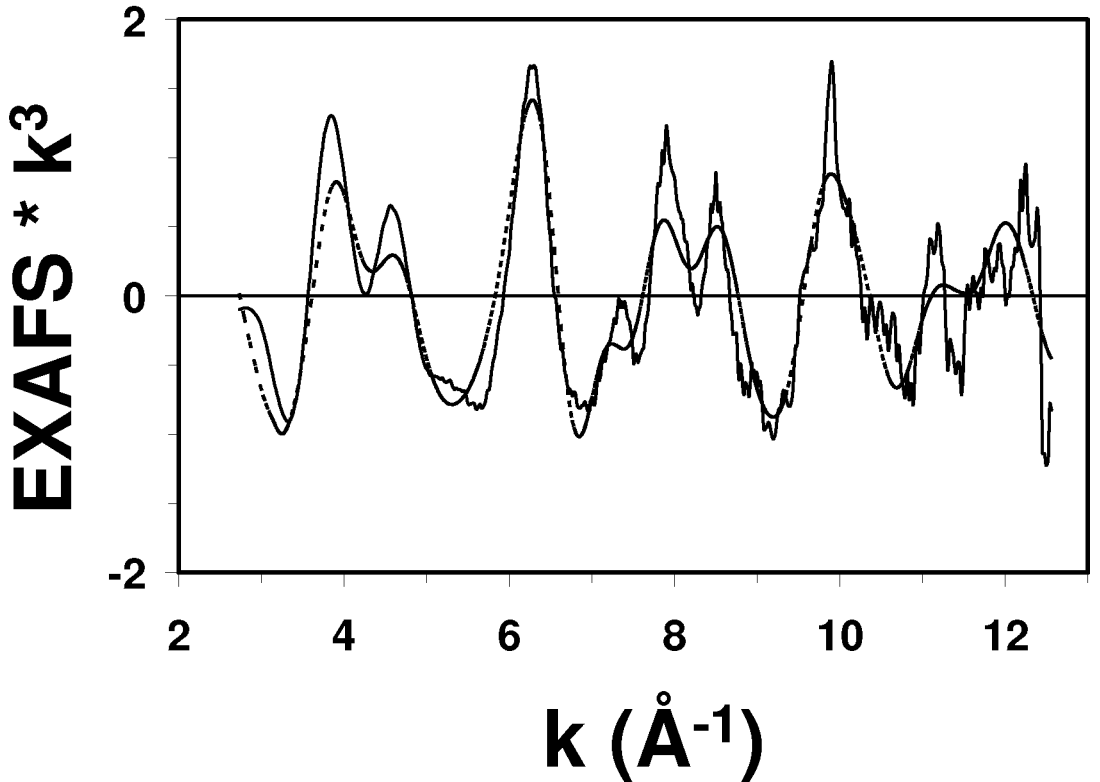

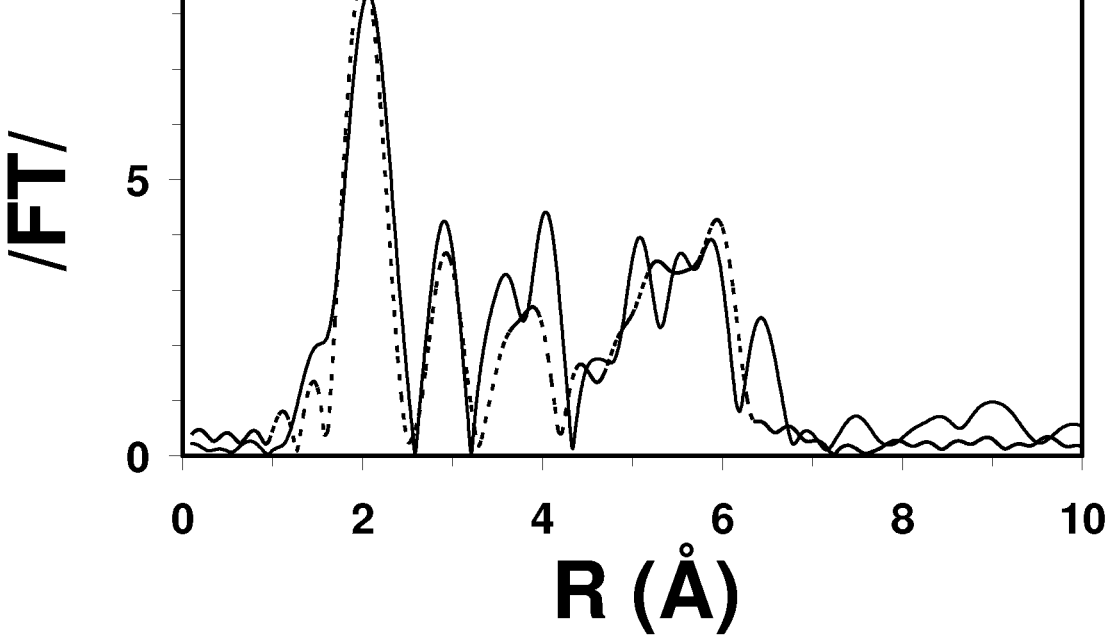
/FT/
5
0
0
2
4
6
8
10
R (Å)

Figure 5e

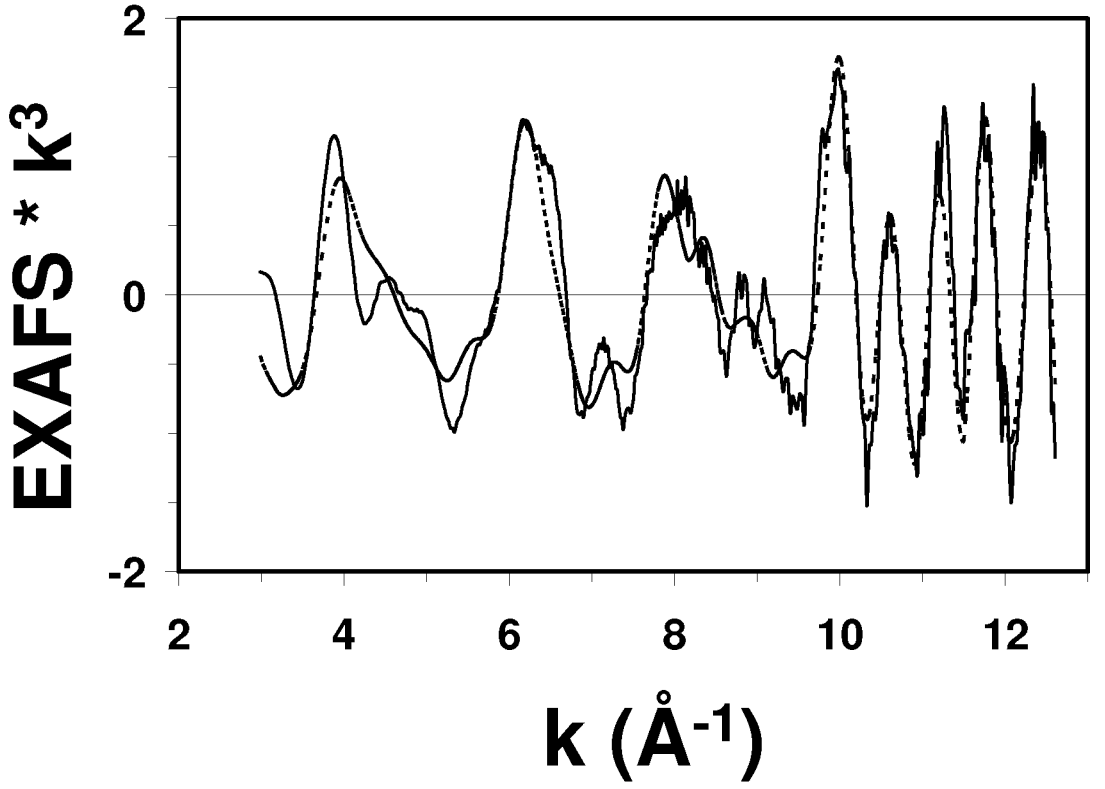

Figure 6

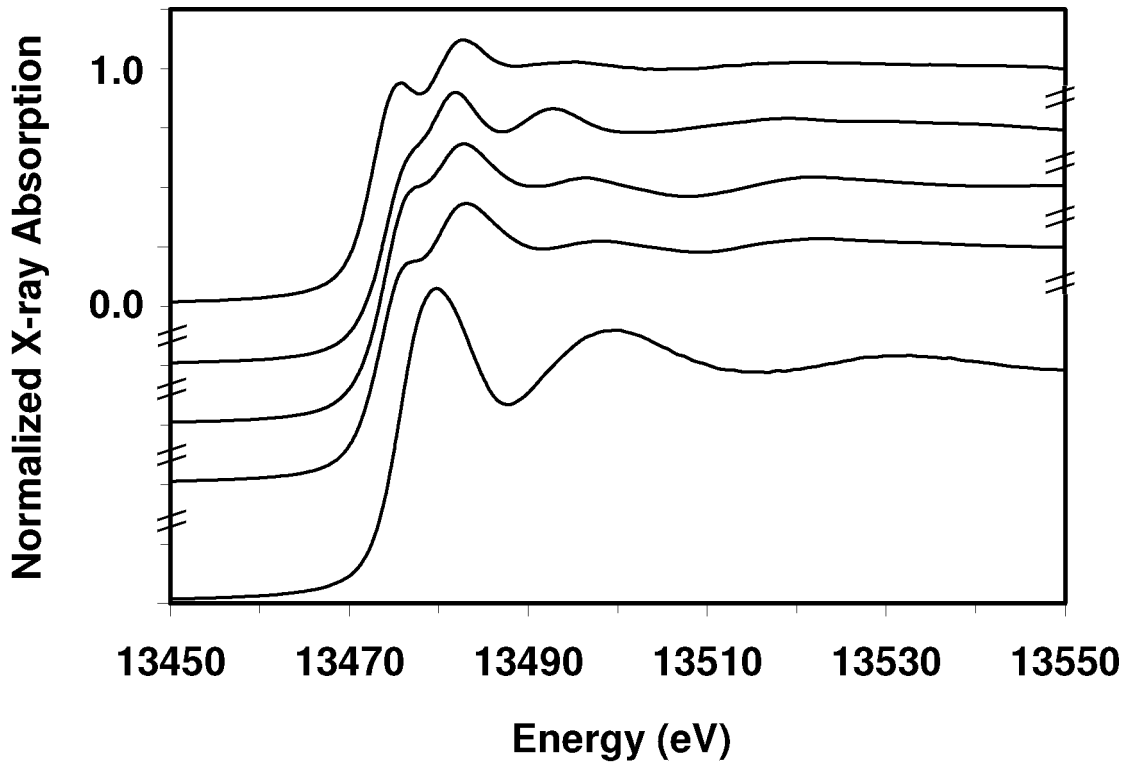
Normalized X-ray Absorption
1.0
0.0
13450
13470
13490
13510
13530
13550
Energy (eV)

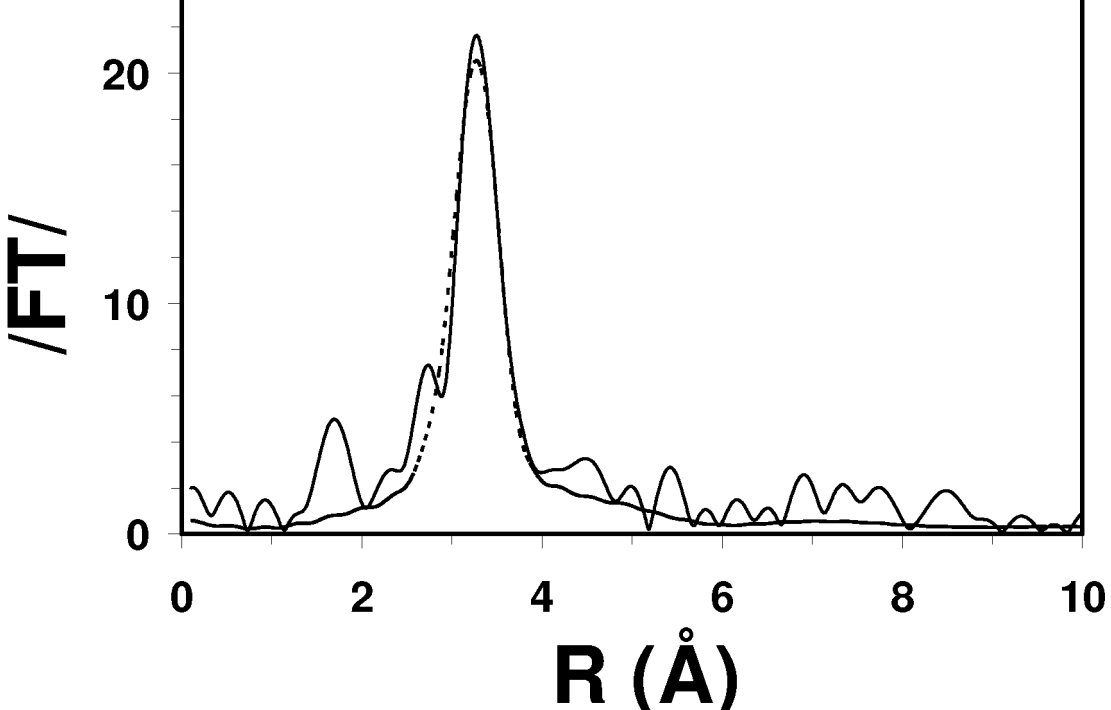
/FT/
20
10
0
0
2
4
6
8
10
R (Å)

Figure 7a

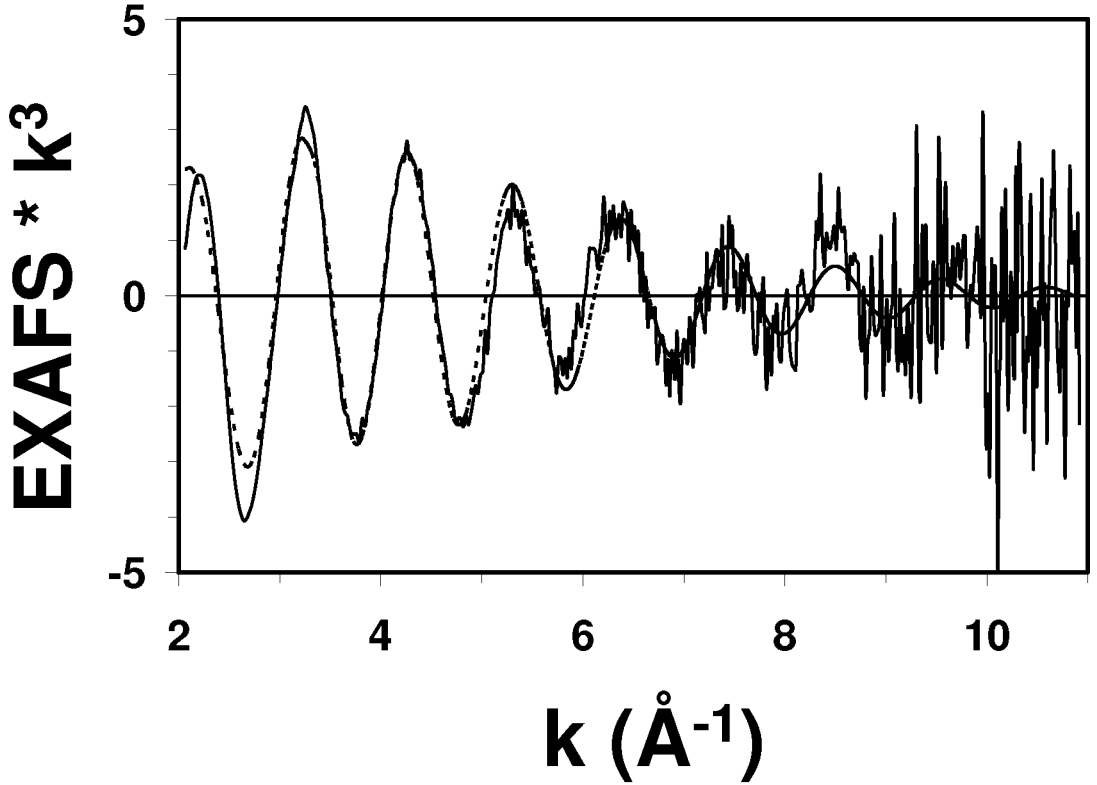

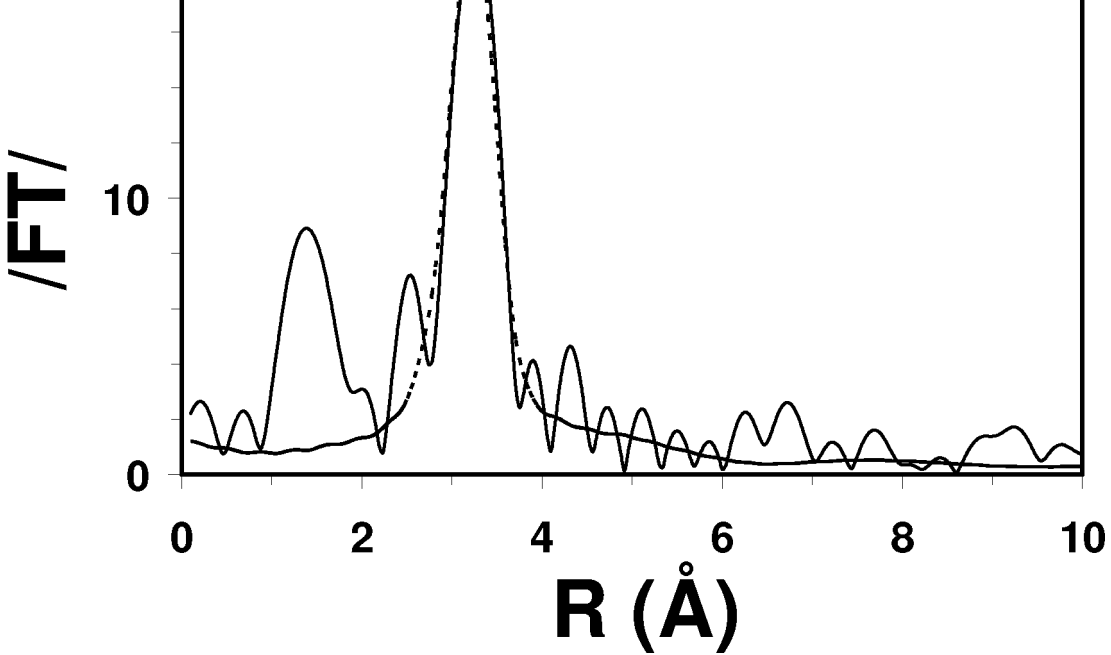
/FT/
10
0
0
2
4
6
8
10
R (Å)

Figure 7b

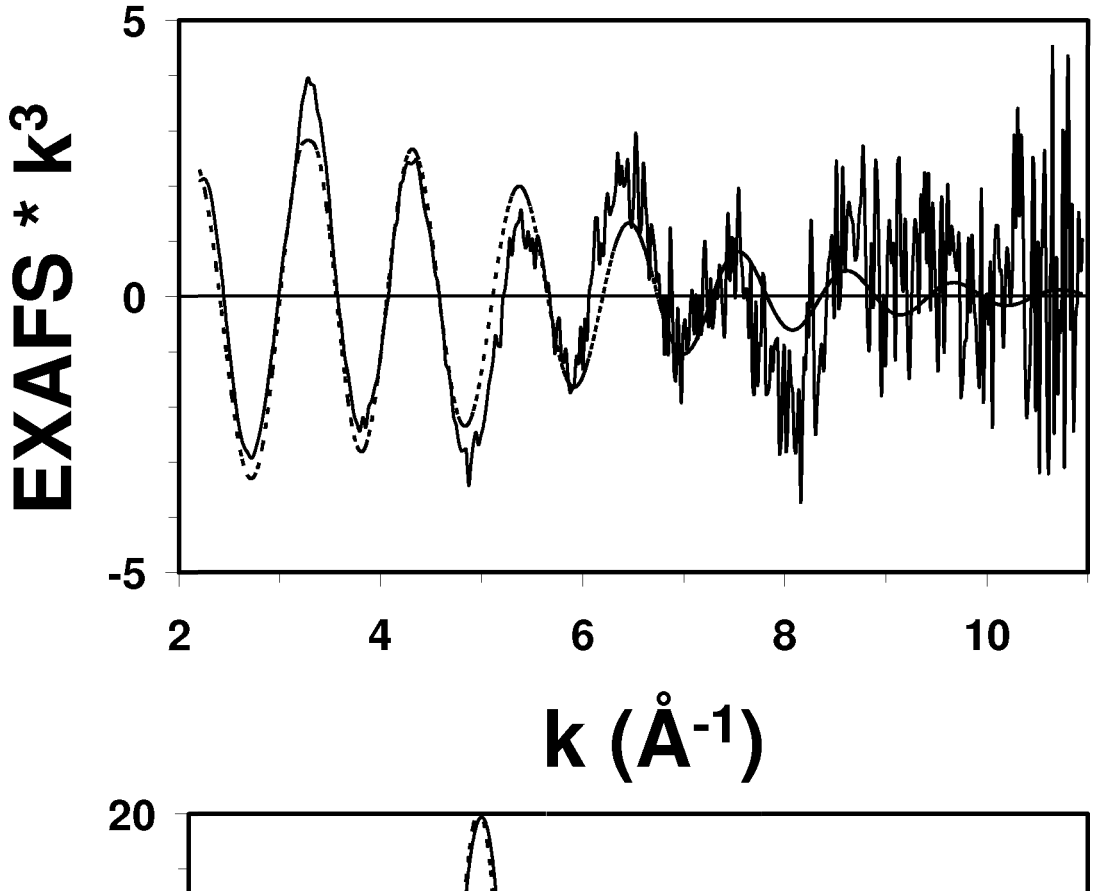

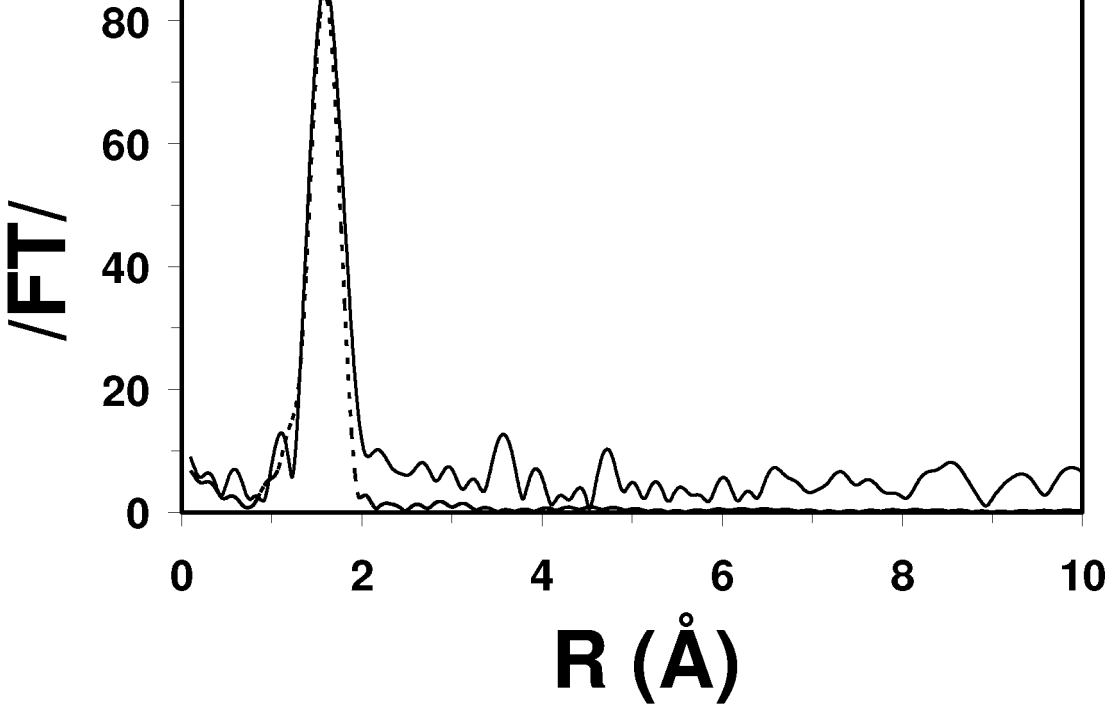
/FT/
80
60
40
20
0
0
2
4
6
8
10
R (Å)

Figure 7c

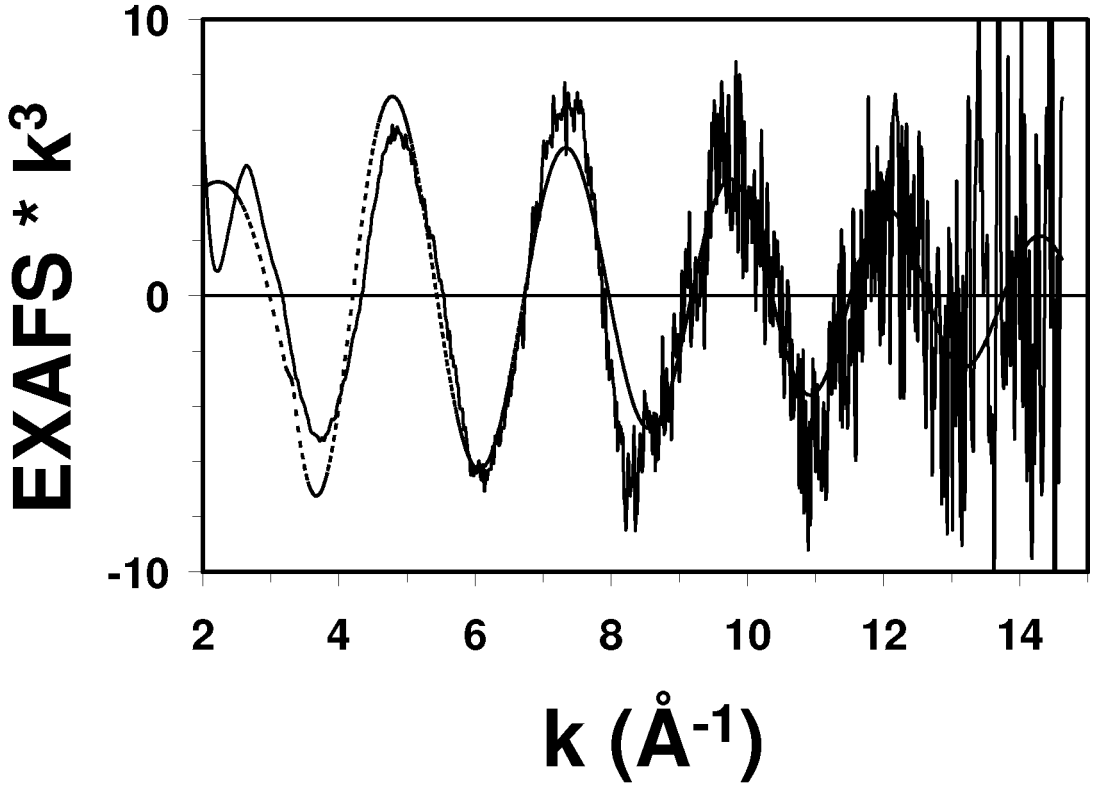

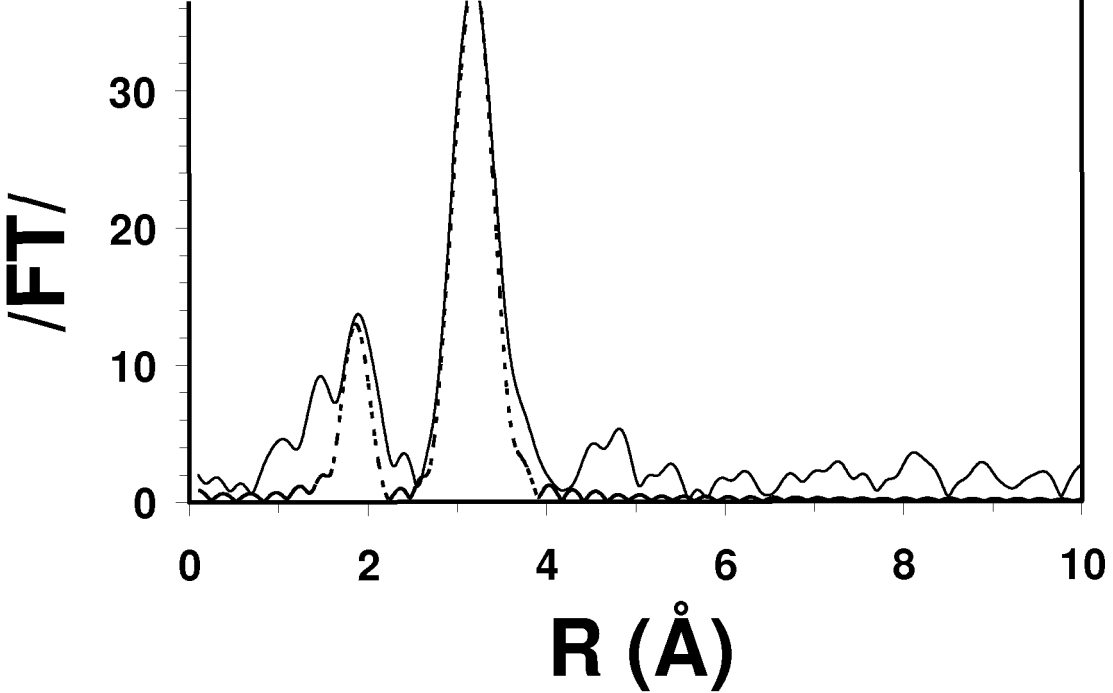
/FT/
30
20
10
0
0
2
4
6
8
10
R (Å)

Figure 8a

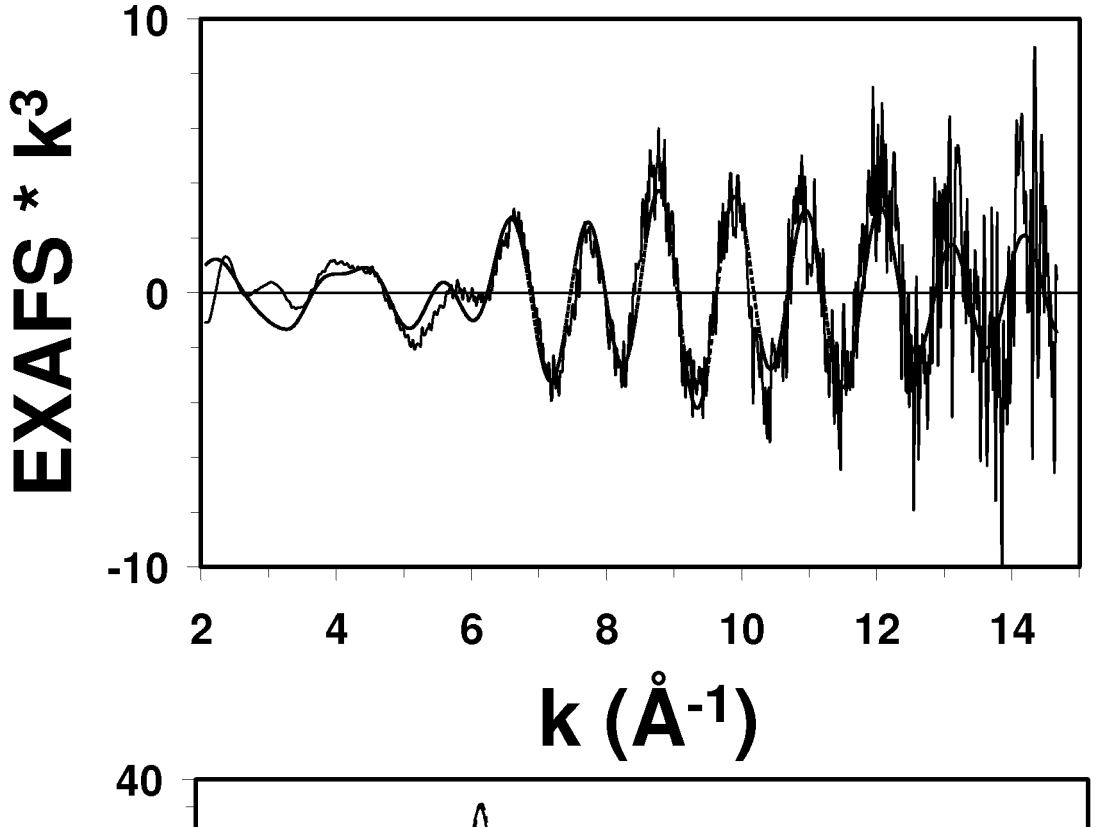

Figure 8b

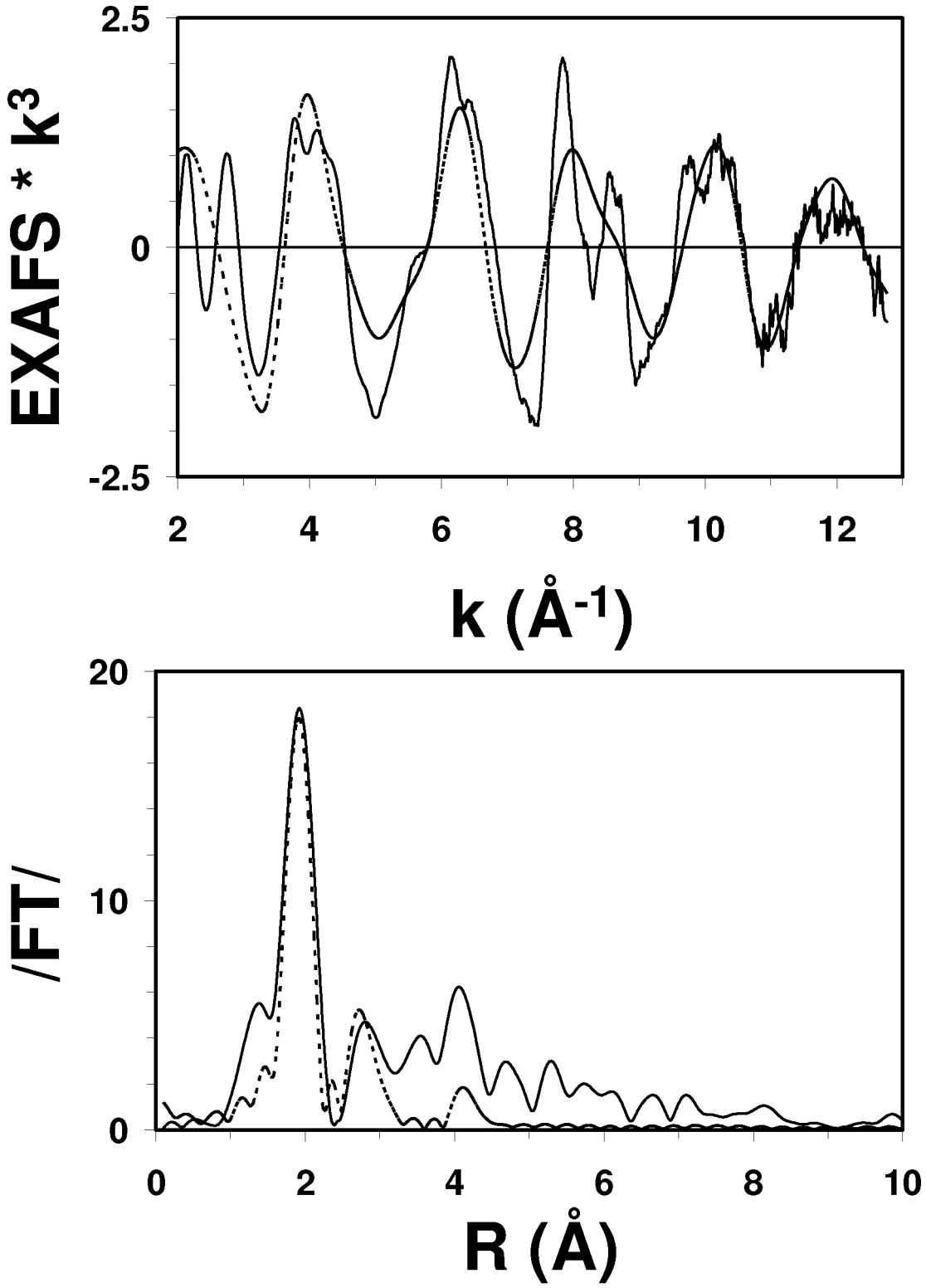

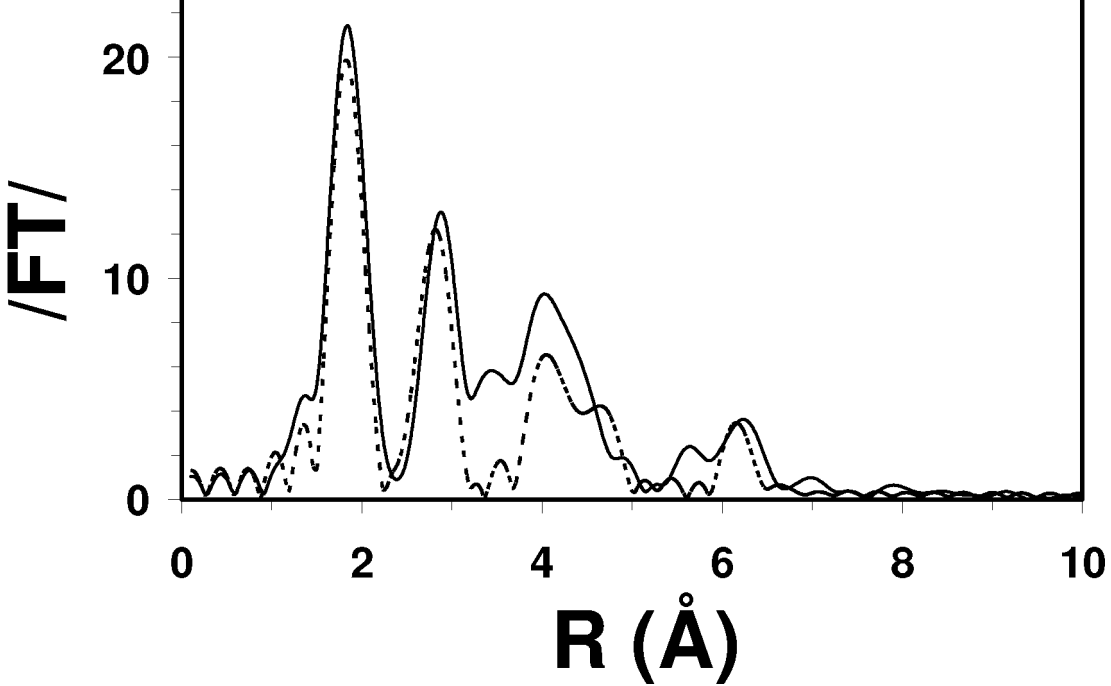
/FT/
20
10
0
0
2
4
6
8
10
R (Å)

Figure 8c

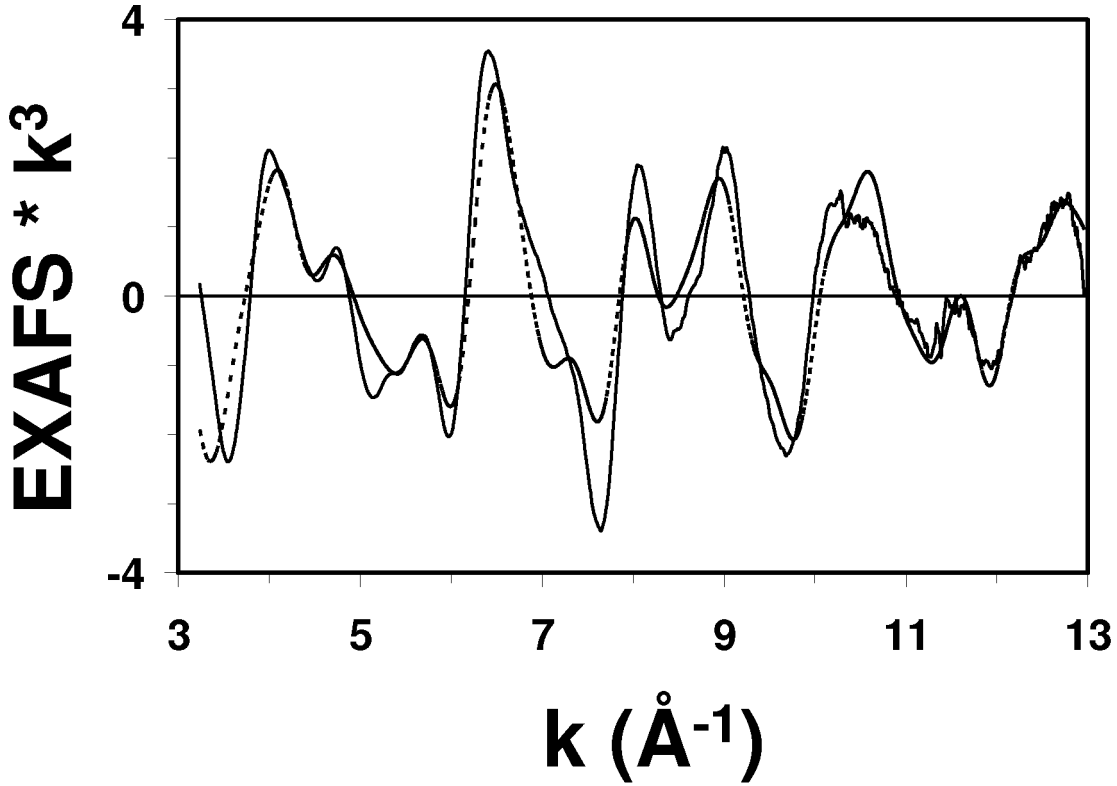

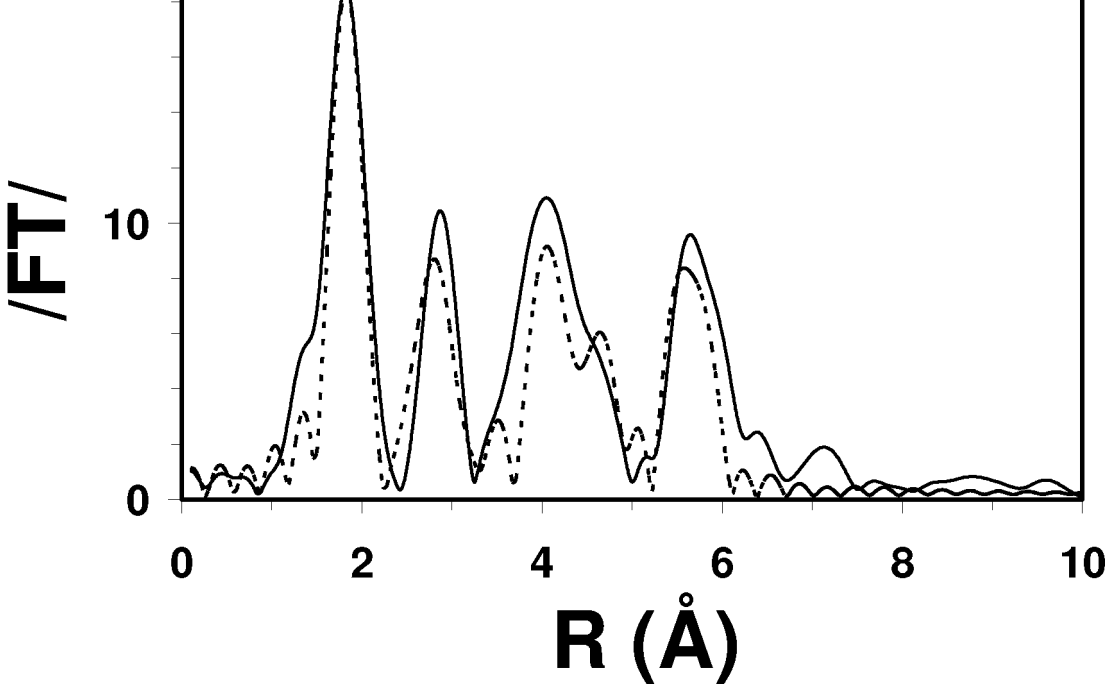
/FT/
10
0
0
2
4
6
8
10
R (Å)

Figure 8d